공학석사 학위논문

Sr-La M-type 육방정 페라이트 합성과 자기적 특성

Synthesis and Magnetic Properties of Sr-La M-type Hexaferrite

2017 년 8 월

서울대학교 대학원

재료공학부

왕 천

Abstract

Since the discovery of $SrFe_{12}O_{19}$ M-type hexaferrite (SrM), $SrFe_{12}O_{19}$ has drawn attention of both researchers and entrepreneurs because of its low production cost, good corrosion resistance, and good magnetic properties. In this study, samples having the compositions of $Sr_{0.5}La_{0.5}Fe_{12-y}O_{19-\delta}$ were synthesized, and the single phase hexaferrites with iron deficiency $0 \leqq y \leqq 0.5$ were obtainable. The effect of iron deficiency on lattice parameters and magnetic properties of hexaferrites were investigated in this study.

Sr-La M-type hexaferrites of $Sr_{0.5}La_{0.5}Fe_{12-y}O_{19-\delta}$ ($-0.25 \leqq y \leqq 2$) were synthesized by solid state reaction. All the precursor powders of La_2O_3, $SrCO_3$, and Fe_2O_3 had 99.9% purity. Precursor powders were weighed, ball-milled for 24 h, and then pressed into pellets. As-pressed pellets were then calcined at 1150, 1200, 1225, 1250, and 1300 °C for 8 h in air, to check if the single phase M-type hexaferrites could be obtained. The calcination was repeated after grinding, ball milling, and pelletizing. As-pressed pellets were put into a muffle furnace and sintered at 1275, 1300 and 1325 °C for 2 h in air. Phases and lattice parameters of sintered samples were analyzed by powder X-ray diffraction (XRD). Field Emission-scanning electron microscopy (FE-SEM) was employed to observe the microstructure. Magnetic properties were measured by a Vibrating Sample Magnetometer (VSM).

Powder XRD patterns indicated that the Sr-La M-type hexaferrites of

$Sr_{0.5}La_{0.5}Fe_{12-y}O_{19-\delta}$ showed well-defined peaks of single phase with a limited range of iron deficiency **y** ($0 \leqq y \leqq 0.5$) after calcination at 1250 and 1300 °C for 8 h in air. When these samples were sintered at 1275, 1300, and 1325 °C for 2 h in air, those samples were not decomposed but still remained as single phase. For the $Sr_{0.5}La_{0.5}Fe_{12-y}O_{19-\delta}$ single phase hexaferrites sintered at 1300 °C, the lattice parameter c and unite cell volumes of the $Sr_{0.5}La_{0.5}Fe_{12-y}O_{19-\delta}$ single phases have the lowest value for the sample with y = 0.25**,** which can be explained by the ionic radius decrease due to the La^{3+} substitution for the Sr^{2+} site of SrM lattice and the ion radius increase from Fe^{3+} to Fe^{2+} ions. The average grain sizes are slightly decreased with increasing the iron deficiency y. The saturation magnetization (M_s) was slightly increased with increasing y compared with pure SrM. The highest M_s value of 72.8 emu/g and coercivity of 3300 Oe were obtained from the $Sr_{0.5}La_{0.5}Fe_{11.5}O_{19-\delta}$ (y = 0.5) samples sintered at 1325 °C for 2 h in air.

In conclusion, single phase is obtainable from $Sr_{0.5}La_{0.5}Fe_{12-y}O_{19-\delta}$ hexaferrites for $0 \leqq y \leqq 0.5$, which have never been reported yet, these may have a promising application in permanent magnet industry since their M_S values are higher than 70 emu/g.

Key Words: magnetoplumbite, iron-deficiency, Sr-La hexaferrites, M-type hexaferrites, solid state reaction, saturation magnetization, coercivity.

Student ID: 2014-25147

Contents

1. Introduction

As a significant member of functional materials, permanent magnetic materials have been widely applied in many major industries [1-3]. With their extension in function and application field, the demand and interest in the permanent magnetic materials are also growing rapidly [4-6]. Up to now, permanent magnet materials went through five stages, the carbon steel, Al-Ni-Co alloy, permanent magnetic ferrites, Sm-Co alloy series, and Nd-Fe-B series. Fig. 1-1 [7] shows the development and the magnetic properties of these five kinds of permanent magnetic materials. Among those materials, the carbon steel production was almost stopped, Al-Ni-Co alloy was widely used in precision instrument due to its extraordinary temperature stability, and Nd-Fe-B magnets were mostly used in some leading-edge equipment, considering both of its amazing magnetic properties and high price; compared to the Nd-Fe-B magnets, Sm-Co magnets have not so good properties but much higher Currie temperature (T_c). Thus, although Sm-Co magnet is expensive, it has promising applications in aerospace and military usage.

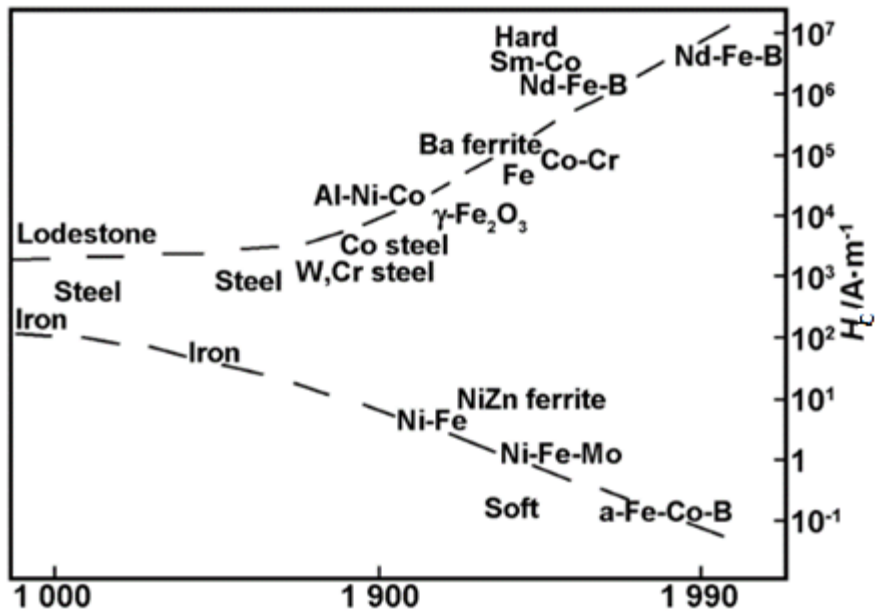

Figure. 1-1 Coercivity change of magnetic materials over time [7]

Ferrites, as part of the permanent magnet material, have high performance-cost efficiency due to their rather cheap raw materials, easier production process, and good magnetic properties [1-4]. The most common raw materials for permanent magnet ferrites are $SrCO_3$, $BaCO_3$, Fe_2O_3, $CaCO_3$, SiO_2, and etc. These oxides and carbonates are stable in air and would not easily have reaction with other chemicals except strong acids. In addition, ferrites have high T_c value of about 450 to 480 °C. Considering these merits, ferrites have a bigger market than rare earth permanent magnetic materials, which have ten times higher magnet energy product than ferrites. In 2012 the production of permanent magnetic ferrites is about 45% of total production of permanent magnetic material, which is 50% bigger than rare earth permanent magnet materials including Nd-Fe-B. So far, permanent magnet ferrites have been not only widely

used in electroacoustic, automation and sound amplifying devices, but also played a very important role in maritime detection, wind-power production, and other industries. As a member of functional material, ferrites have a positive impact on the new energy industry, which means that they are national strategic resources for both Korea and China.

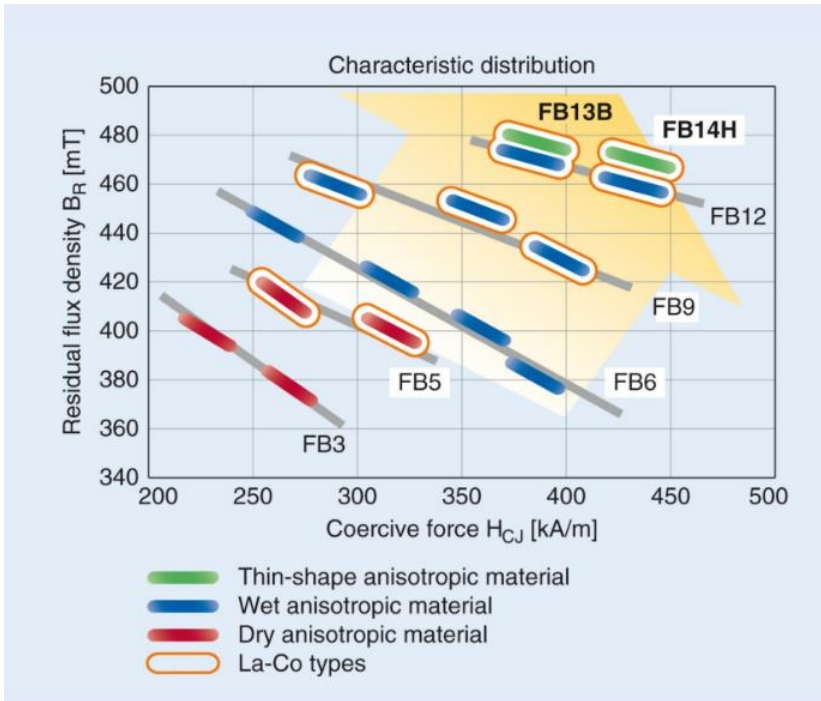

Figure.1-2 Magnetic properties of sintered magnet products of TDK [9]

Compared to BaM hexaferrites, SrM hexaferrites have slightly higher magnetic properties. The nominal composition of SrM is $SrFe_{12}O_{19}$, or $(SrO)\cdot 6(Fe_2O_3)$. One unit cell of SrM lattice consists two SrM molecules, and the ions are isolated by ten layer of O^{2-} ions. Spinel (S, Fe_6O_8) and hexagonal (R, $SrFe_6O_{11}$) blocks comprise the SRS*R* structure, forming the microstructure of hexaferrites where * represents a 180° rotation around the hexagonal c-axis. 24

Fe^{3+} ions are distributed on five different sites, three in hexagonal sites (12k, $4f_2$ and 2a), one tetrahedral site ($4f_1$), and one hexahedral site (2b). In which 12k, 2a and 2b sites are spin up while $4f_1$ and $4f_2$ sites are spin down to align parallel with the crystallographic c-axis, which thus give BaM a net magnetic moment of $20\mu_B$. SrM ferrites have a slightly higher value of $20.6\mu_B$ [6].

To increase the magnetic properties of SrM, many methods have been attempted, one effective method is to use rare earth element ions for the substitution of the Sr^{2+} ions because Sr^{2+} ion radius is 0.127 nm close to the O^{2-} ion radii of 0.132 nm, so that Ca^{2+}, Na^{+} and K^{+} ions and rare earth element ions can partially or completely substitute the Sr^{2+} ions. According to the Mössbauer spectroscopy, La^{3+} substitution could make Fe^{3+} turns to Fe^{2+} in 2a sites [1], which is helpful for stabilization of magnetoplumbite structure. Y.F. Wang et al. [8] reported that iron deficiency facilitates the formation of single phase SrM hexaferrites. High performance hexaferrites with great properties were commercialized by Japan companies such as TDK (Fig.1-2) [9].

In this study, ferrites of Sr-La M-type were synthesized by conventional solid state method with an iron deficiency factor y to enhance the ionic diffusion and improve the related magnetic properties. We report the effect of iron deficiency on Sr-La hexaferrites microstructure and magnetic properties.

2. Background

2.1. Crystal structure of M type hexaferrites

The nominal composition of SrM is $SrFe_{12}O_{19}$, or $(SrO)\cdot 6(Fe_2O_3)$. There are three kinds of most commonly used ferrites classified by their crystal structures, spinel, garnet and hexaferrites. M-type hexaferrites have the simplest structure among the hexaferrites, such as the W-type. M–type permanent magnetic ferrites have magnetoplumbite structure as Fig. 2-1 showed., BaM ($BaFe_{12}O_{19}$) and SrM ($SrFe_{12}O_{19}$) are the representatives of M-type hexaferrites. A unit of SrM lattice consists two SrM molecules and the ions is isolated by ten layers of O^{2-} ions. Spinel (S, Fe_6O_8) and hexagonal (R, $SrFe_6O_{11}$) blocks comprises in the form of SRS*R*, forming the microstructure of SrM hexaferrites. There are four octahedrons, two tetrahedrons in a S-block and one hexahedron, five octahedrons in a R-block. In these blocks, Fe^{3+} ions exist in the interface of O^{2-} ions, Sr^{2+} replaced the positions of O^{2-} ions, and make a stable hexagonal structure. However, SrM ferrites are different from other ferrites that because of they have a strong anisotropy along the c-axis, which lead to a strong magnetic anisotropy. The theoretical lattice parameters for SrM ferrites are a = b = 5.892 Å, c = 23.183 Å [6], and an a/c ratio of 3.93. 24 Fe^{3+} ions are distributed on five sites, three in hexagonal sites (12k, $4f_2$ and 2a), one tetrahedral site ($4f_{1)}$ and one hexahedral site (2b). In which 12k, 2a and 2b sites are spin up because of super-exchange while $4f_1$ and $4f_2$ sites are spin down to align parallel with the crystallographic c-axis, thus give SrM a net magnetic moment of $20\mu_B$. The experiment result of

SrM is 20.6μ_B at 0K, which is close to the theoretical value.

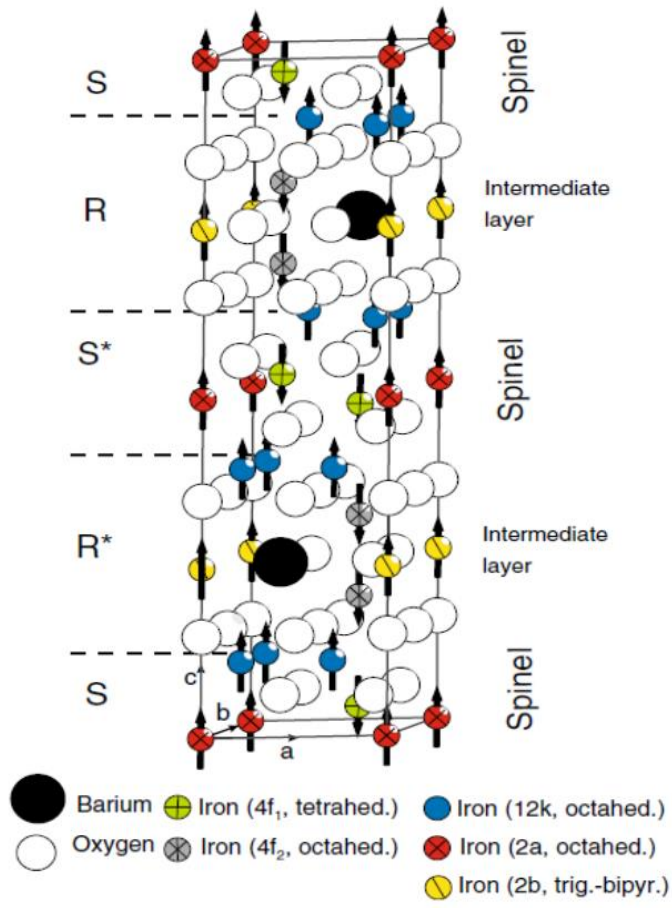

Figure. 2-1 Crystal structure of M-type hexaferrites [10]

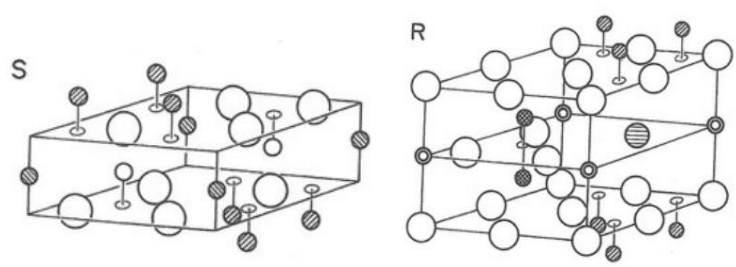

Figure. 2-2 Perspective drawing of S block (left) and R block (right) [6].

2.2 Magnetic properties of M type hexagonal ferrites

2.2.1 Saturation magnetization M_s and remanence M_r

Hysteresis loop is a curve to show the relationship between the magnetization M or applied magnetic field B with magnetic field strength H when a sample was magnetized repeatedly as showed in Fig. 2-3.

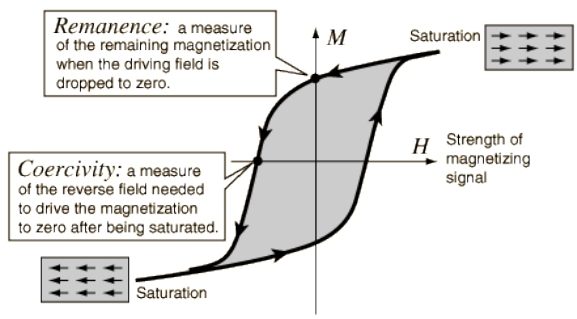

Figure. 2-3 the magnetic hysteresis loop [11]

Saturation magnetization (M_s) is a state at which an increasing applied external magnetic field H cannot increase the magnetization of the material anymore, so the total magnetic flux density B more or less levels off. When a magnet reaches its saturation magnetization, all domains are lined up with the growing field, favorably oriented domains replaces the unfavorably oriented domains and rotation completes the alignment of the domains with the field. It is closely related to the compositions, domain and crystal structures of the materials.

Remanence, or remnant magnetization or residual magnetism (M_r) is the magnetization residual left in a ferromagnetic material (such as iron) after an

external magnetic field was removed, it depends on the properties, compositions and structures of the materials, and it is also an important factor to judge if it is a permanent magnet. The remanence of magnetic materials provides the magnetic memory in magnetic storage devices, and is used as a source of information on the Earth magnetic field in paleomagnetism in the past.

The molecular magnetic moment from a molecule of $SrFe_{12}O_{19}$ occupying half of the unit cell, consists of SRS*R* blocks which contain two $SrFe_{12}O_{19}$ molecules. Fe^{3+} ion magnetic moment of $5\mu_B$, thus the theoretical molecular magnetic moments values are as follows (2-1):

$$M_s\,(T) \;=\; M_{2a}(T) + M_{2b}(T) + 6M_{12k}(T) - 2M_{4f_1}(T) - 2M_{4f_2} \qquad (2\text{-}1)$$

$$M_s = 5 \times (6 + 1 + 1 - 2 - 2) = 20\mu_B,$$

The results fits with the theoretical result of SrM ($20.6\mu_B$) at 0K. [6]

2.2.2 Coercivity H_c

The coercivity (H_c), also so-called the magnetic coercivity, coercive field or coercive force, is a measure of the resistance of a magnetic material to change in magnetization, equivalent to the field intensity necessary to demagnetize the fully magnetized material.

In most cases the remanence and coercivity are two properties against each other. That is because that $M_r = M_s \cdot \cos\boldsymbol{\theta}$, and H_c is in inverse proportion to M_s. So it is important to increase M_s without obvious decrease of H_c which is closely related to the magnetocrystalline anisotropy (MCA) and grain size.

2.2.3 Magnetocrystalline anisotropy

Anisotropy is the property of being directionally dependent, which implies different properties in different directions, as opposed to isotropy.

The magnetocrystalline anisotropy is a special case of magnetic anisotropy. if a material takes more energy to magnetize it in certain directions than in others, then we can say it have magnetocrystalline anisotropy. These directions are usually related to the principal axes of its crystal lattice, for SrM, the c-axis [0001].

The magnetocrystalline anisotropy describes the difficulty to be magnetized for a magnetic material in different directions. Magnetocrystalline anisotropy is the main reason for SrM hexaferrites have such good magnetic properties, thus it is an important parameter for hexagonal ferrites, as shown in equation (2-2) [11]:

$$E_K = K_0 + K_1 \sin^2\theta + K_2 \sin^4\theta + K_3 \sin^6\theta \cdot \cos^6\phi \qquad (2\text{-}2)$$

In which θ is the angle between the c-axis and the direction of magnetization, K_0 means the energy to magnetize the easy axis. ϕ is the azimuthal angle of M_s projected in the plane perpendicular to the hexagonal axis [0001]. Generally, we only deal with the terms associated with θ. In the hexagonal ferrites cases of three magnetocrystalline anisotropy constants, generally, the equation (2-2) is only accurate to the quadratic term of $\sin\theta$, so that the equation (2-2) can be simplified as (2-3):

$$E_K = K_0 + K_1 \sin^2\theta + K_2 \sin^4\theta \qquad (2\text{-}3)$$

There are three easy magnetization directions for MCA because the difference of K_1 and K_2 and sizes, (1) Parallel to the easy axis - hexagonal axis [0001]; (2) Parallel to the easily magnetized plane - perpendicular to the [0001] axis; and (3) Forming a conical plane with an angle to [0001].

2.3. Cation substitution of M type hexaferrites

Since the application of SrM ferrites permanent magnet in 1950s, the properties of SrM was improving gradually. There are mainly two kinds of methods to improve the magnetic properties of hexaferrites, technological controls and ion substitution. It is not enough to just control the factors such as ball milling time, ratio of ball to raw material, calcination and sintering temperature, heat preservation time and pressing quality, Reports indicated that by substitution of certain ions in ferrites, the magnetic properties can be improved to the next level, and some of them even reached the theoretical value, in this case, ion substitution is a very effective method for magnetic property improvement of hexaferrites.

2.3.1 Me substitution in M type hexaferrites

Judging by the crystal structure and magnetic moment source, the most common used method for $MeFe_{12}O_{19}$ substitution is the Me ions substitution, which lead to a more stable crystal structure, stronger magnetic anisotropy and thus more excellent magnetic properties. In SrM ion substitution, elements with similar ion radii to Sr^{2+} are first to be considered, such as Ca^{2+}, La^{3+}, K^{+}, Rb^{+}, and etc. Many studies investigated that the substitution of rare earth ions improving the performances of ferrites materials [12]. Lotgering [13] studied the La^{3+} completely substitution of Sr^{2+}, the experiment result showed that the product $LaFe_{12}O_{19}$ was companied with minor Fe3O4 and LaFeO3 second phases and had

a very high anisotropy constant. At T = 0 K the value of K_1 is 19 to 24×10^5 erg/g, which is much bigger than BaM at T = 0K. It is also proved that the extraordinary MCA constant was because the Fe^{3+} have a valence change to Fe^{2+} and occupied the 2a sites. The reason for the improvement is that the rare earth element ions have a close packed double hexagonal crystal structure thus lead to the strong magnetic anisotropy.

Lei *et al*. reported La^{3+}substitution via molten salt assisted sintering, the La ratio was no more than 0.2[14], Lechevallier *et al*. investigated the formation of Sr-Sm Hexaferrites and enhanced the magnetic properties [15].

2.3.2 Fe ion substitution in M type hexaferrites

Fe^{3+} ions occupied five different crystal sites, 2a, $4f_2$, and 12 k, $4f_1$ and 2b for SrM, in which $4f_1$ and $4f_2$ sites magnetic moments orientation is spin down thus weaken the net magnetic moments of the hexaferrites. Therefore, researchers have attempted some non-magnetic ions to substitute the magnetic iron ions such as Co^{3+}, Cr^{3+}, Al^{3+} at the $4f_1$, $4f_2$ position. For instance, when an Co^{3+} ion ($3.7\mu_B$) substitutes Fe^{3+} ion ($5\mu_B$) at $4f_2$ site, substitution can increase the net magnetic moment to a certain degree to get more Bohr magnetic number and lead to increase saturation magnetization [16].

2.3.3. Ion co-substitution in M type hexaferrites

People found out that by La-Co co-substitution method, high quality ferrites permanent magnet could be synthesized in 1996. Nowadays, the study on ion

co-substitution is much more popular compared to single substitution of Me ion or Fe ion before.

Many study have been done on La^{3+}-Co^{2+} co-substitution and reported increasing in H_c without reducing the M_s [17]. P.Tenaud, Kools, Lechevallier *et al*. [18-21] investigated the effect of different La^{2+} and Co^{2+} substitution ratio on SrM, the experiment results indicated that the ideal substitution ratio for $Sr_{1-x}La_xFe_{12-y}Co_yO_{19-\delta}$ hexaferrites is x=y=0.2 when La^{2+} and Co^{2+} mole number are equal, and when y/x= 0.75 the best magnetic properties was achieved. Co^{2+}-Ti^{4+} co-substituted Fe^{3+} induced decrease of the coercivity without change of saturation magnetization.

3. Experimental

3.1 Synthesis of Sr-La hexaferrites

In this study, Sr-La M-type hexaferrites (SrLaM) powder with the compositions of $Sr_xLa_{1-x}Fe_{12}O_{19}$ (x = 0.4, 0.5, 0.6) and $Sr_{0.5}La_{0.5}Fe_{12-y}O_{19-\delta}$ (y = 0, 0.25, 0.5) were synthesized by conventional ceramic method (solid state reaction). Purity for all the raw powders of La_2O_3, $SrCO_3$, Fe_2O_3 were 99.9%. Raw powders were processed by weighting and ball-milling for 24 h in a plastic container with zirconia balls and ethanol (99.99%). The ball with three different radii have the weight ratio 5:3:2. The mixture was then dried in oven at 60 °C, ground, and sieved to 100 mesh. Precursor Powders were pressed to pellets with a two-inches mold. Pellets were calcined at 1150, 1200, 1225,1250, 1300 °C for 8 h in air. The calcination was repeated again by intermediate ball milling and pelletizing. The second calcinations were performed to complete solid state reaction and achieve compositional homogeneity of the samples. These calcined powders were pressed for pellets which later were sintered at 1275, 1300, 1325 °C, for 2 h in air.

3.2 Characterization

3.2.1 X-ray diffractometer (XRD) analysis of crystallinity and phases of $Sr_xLa_{1-x}Fe_{12}O_{19}$ hexaferrites ($0.4 \leqq x \leqq 0.6$) and $Sr_{0.5}La_{0.5}Fe_{12-y}O_{19-\delta}$ hexaferrites ($-0.25 \leqq y \leqq 2$)

X-ray diffractometer was employed to obtain X-ray diffractograms of SrM ferrites with different Sr/La ratio and iron deficiency. $Sr_xLa_{1-x}Fe_{12}O_{19}$($0.4 \leqq \boldsymbol{x} \leqq 0.6$) and $Sr_{0.2}a_{0.5}Fe_{12-y}O_{19-\delta}$ ($-0.25 \leqq \boldsymbol{y} \leqq 2$) were analyzed by X-ray diffractometer (Bruker Miller Co.D8-advance). XRD was using Cu Kα1 with a wave length of 1.54056 Å, voltage and current were set to 40 kV and 40 mA.

3.2.2 Microstructure observation using field emission scanning electron microscopy (FE-SEM)

FE-SEM (JEQL, JSM-6330F) was used to observe the microstructures of samples. Polishing and chemical etching were processed before SEM for better observation of microstructure. The etching condition of the sample was treated with a 35% HCl acid at 70 °C for 120 seconds.

3.2.3 Measurement of magnetic properties

Magnetic properties were measured at room temperature with vibrating sample magnetometer (VSM-7410). The maximum applied field of 25 kOe was used to evaluate the magnetic properties.

3.2.4 Measurement of sintered density

The sintered density is measured using the Archimedes method. First, the sintered samples were immersed in distilled water and boiled for 1 h. After removing distilled water in pores at the surface, the weight W_{sat} and W_{fluid} were weighted, respectively. Then samples were dried for 2 h and then the weight in the air W_{air} was measured. The experimental density (ρ_1), theoretical density (ρ_2) and relative density ($\rho_{\%}$) was calculated by the equation (3-1), (3-2) and (3-3) as follows:

$$\rho_1 = \frac{W_{air}}{(W_{sat} - W_{fluid})} \qquad (3\text{-}1)$$

$$\rho_2 = \frac{2M}{NV_{cell}} \qquad (3\text{-}2)$$

$$\rho_{\%} = \frac{\rho_1}{\rho_2} \qquad (3\text{-}3)$$

(M: molecular weight, N: Avogadro constant, V_{cell}: unite cell volume)

4. Result and Discussion

4.1 Crystal structure of $Sr_xLa_{1-x}Fe_{12}O_{19}$ ($0.4 \leqq x \leqq 0.6$)

Fig.4-1(a), 4-1(b) and 4-1(c) showed X-ray diffraction (XRD) patterns of the calcined powders of $Sr_{1-x}La_xFe_{12}O_{19}$ (x=0.4, 0.5 and 0.6) with varying temperature from 1150 to 1300 °C for 8 h in air. The XRD patterns of x = 0.4 at calcination temperature above 1200 °C (Figure 4-1(a)) and x = 0.5 at above 1250 °C (Figure 4-1(b) showed single phase M-type hexagonal structure. In such conditions, no obvious characteristic diffraction peaks of $LaFeO_3$ and Fe_2O_3 could be found from the XRD patterns, indicating that those ions entered the SrM lattice without forming second phases. No single phase hexaferrites were obtained when x = 0.6 (Fig.4-1(c)). The results were listed in Table 4-1.

Wang *et al*. explored the solubility of rare earth ion in SrM is very low and their introduction tend to the secondary phases [22]. Since studies on ferrites with La ratio x no more than 0.4 have been widely reported, D.seifer *et al* .also reported at 1300 °C La have the maximum solubility of 0.5[13], so that the La ratio was fixed at x=0.5 to check the effect of iron deficiency on phase conditions on $Sr_{0.5}La_{0.5}Fe_{12-y}O_{19-\delta}$ hexaferrites.

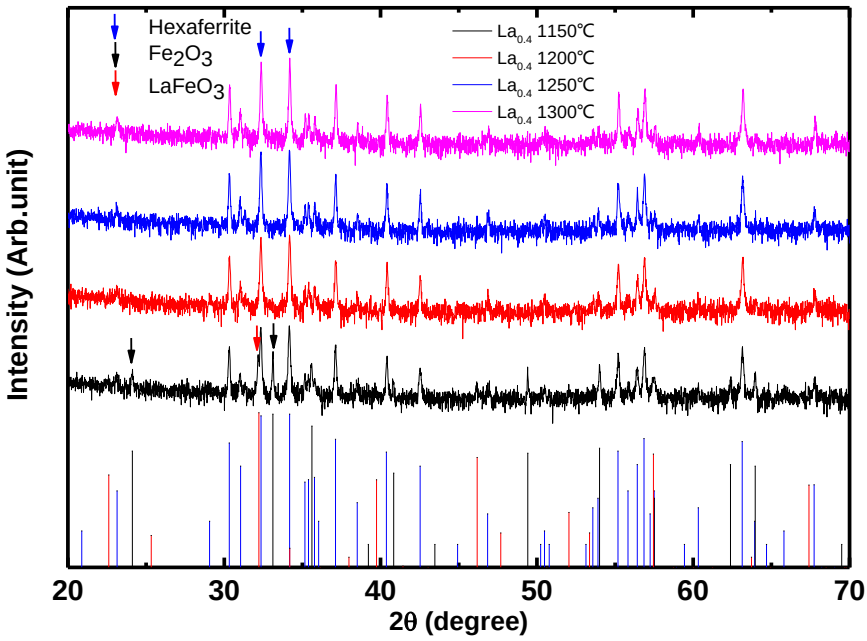

Figure. 4-1(a) XRD patterns of $Sr_{0.6}La_{0.4}Fe_{12}O_{19}$ calcined in air

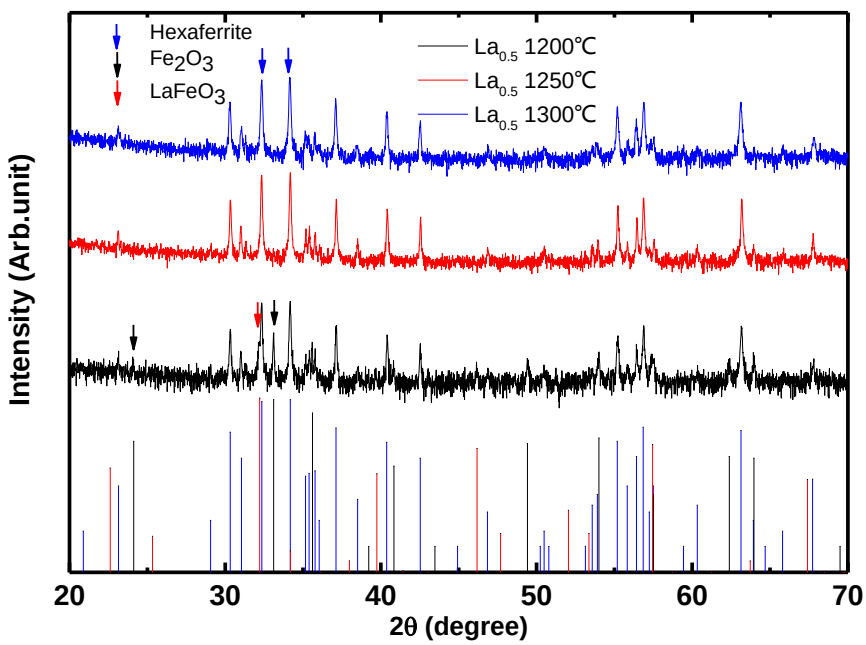

Figure.4-1(b) XRD patterns of $Sr_{0.5}La_{0.5}Fe_{12}O_{19}$ calcined in air

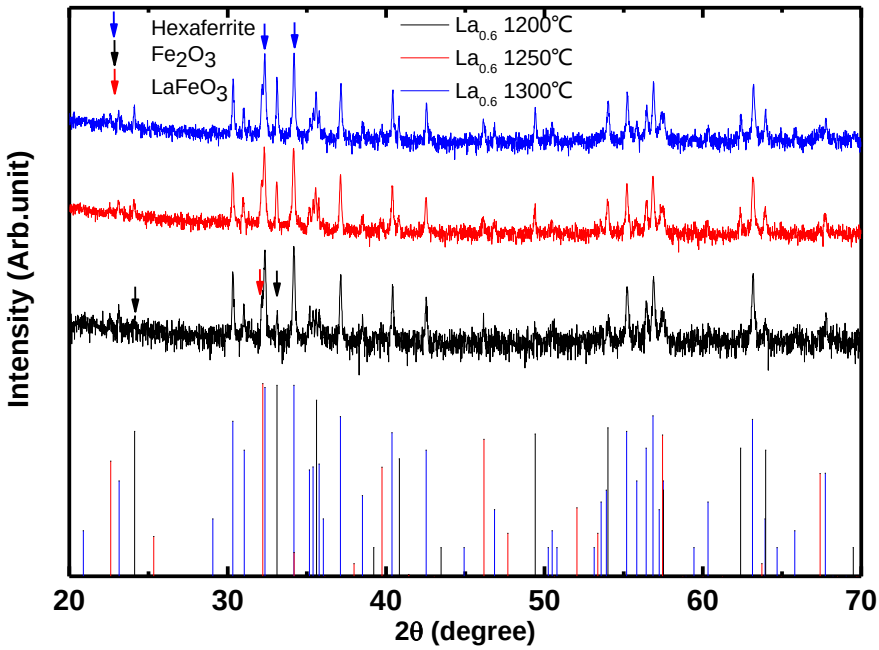

Figure. 4-1(c) XRD patterns of $Sr_{0.4}La_{0.6}Fe_{12}O_{19}$ calcined in air.

Table 4-1 Detected phases from XRD patterns of

$Sr_{1-x}La_xFe_{12}O_{19}$ after calcination in air

Temperature (℃) / Composition.x	1150	1200	1250	1300
x=0.4	M+F+L	M	M	M
x=0.5	-	M+F+L	M	M
x=0.6	-	M+F+L	M+F+L	M+F+L

M: SrM F: Fe_2O_3 L:$LaFeO_3$

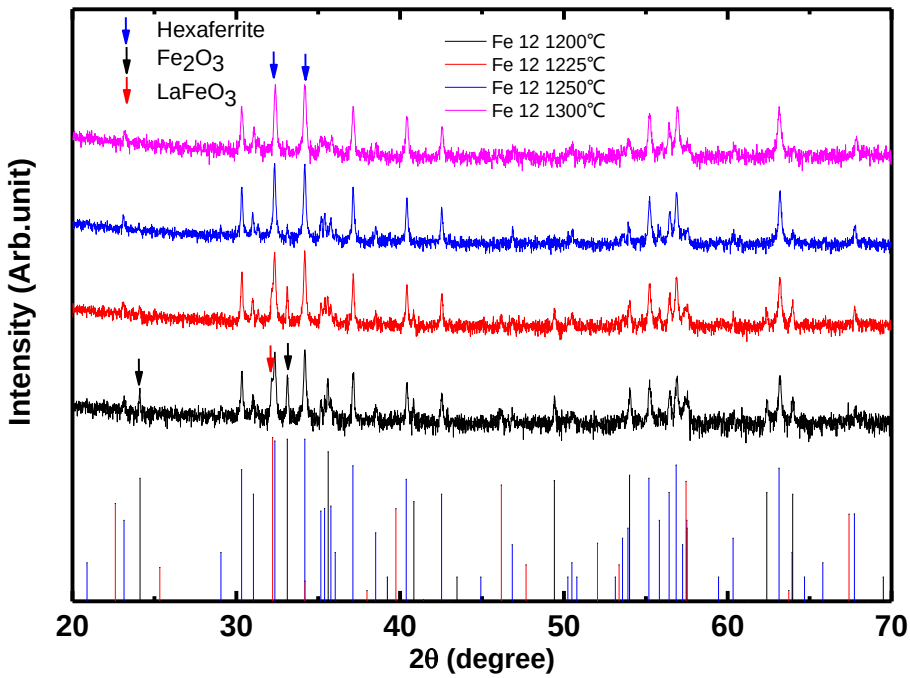

Figure. 4-2(a) XRD patterns of $Sr_{1-x}La_xFe_{12.25}O_{19-\delta}$ calcined in air.

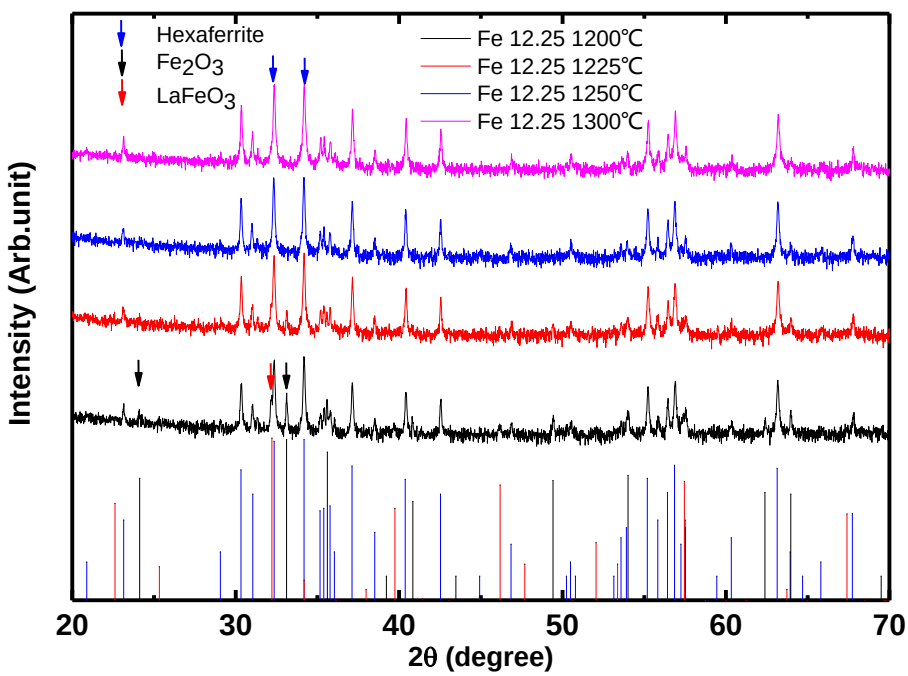

Figure. 4-2(b) XRD patterns of $Sr_{1-x}La_xFe_{12}O_{19-\delta}$ calcined in air.

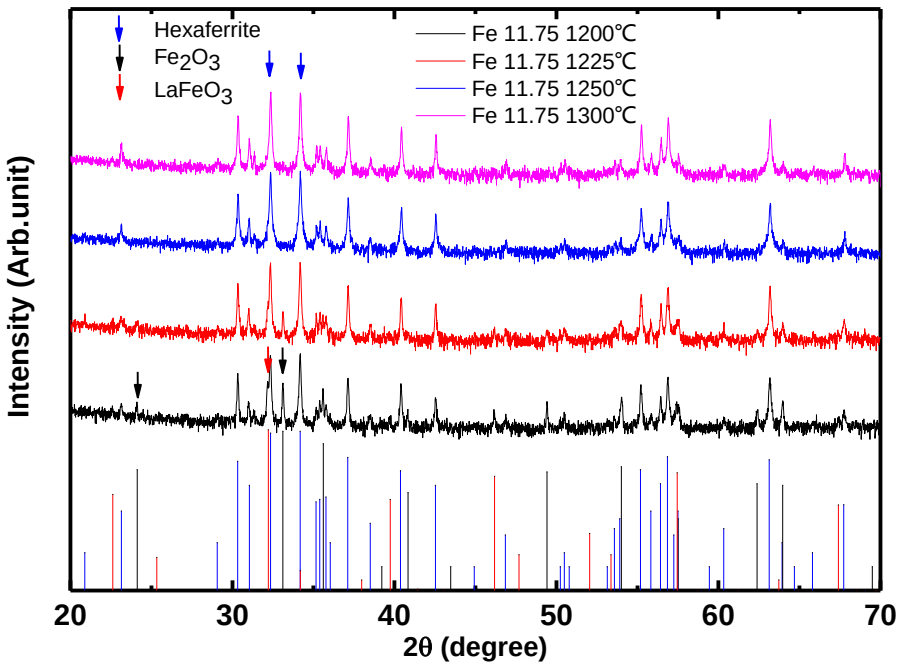

Figure. 4-2(c) XRD patterns of $Sr_{1-x}La_xFe_{11.75}O_{19-\delta}$ calcined in air.

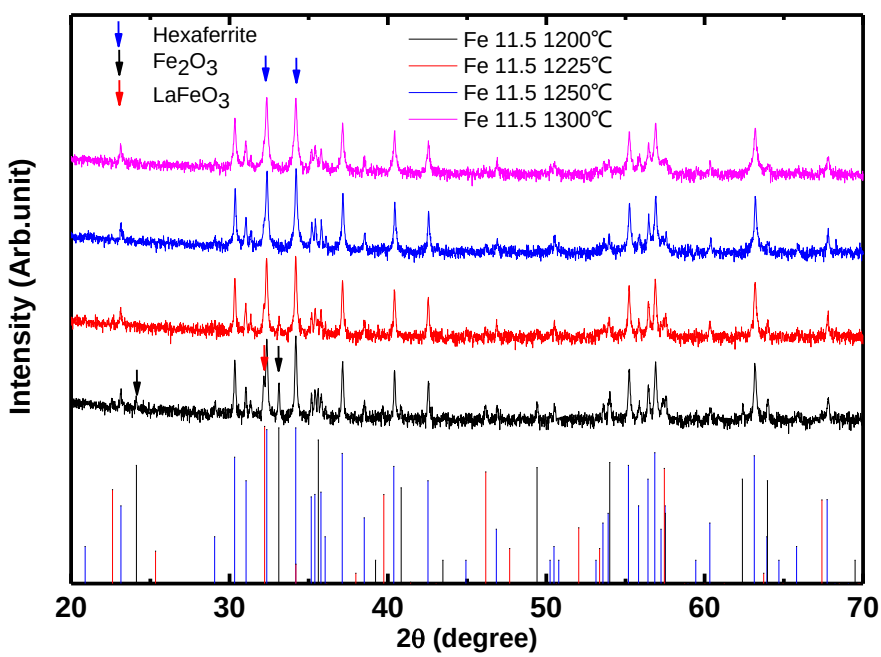

Figure. 4-2(d) XRD patterns of $Sr_{1-x}La_xFe_{11.5}O_{19-\delta}$ calcined in air

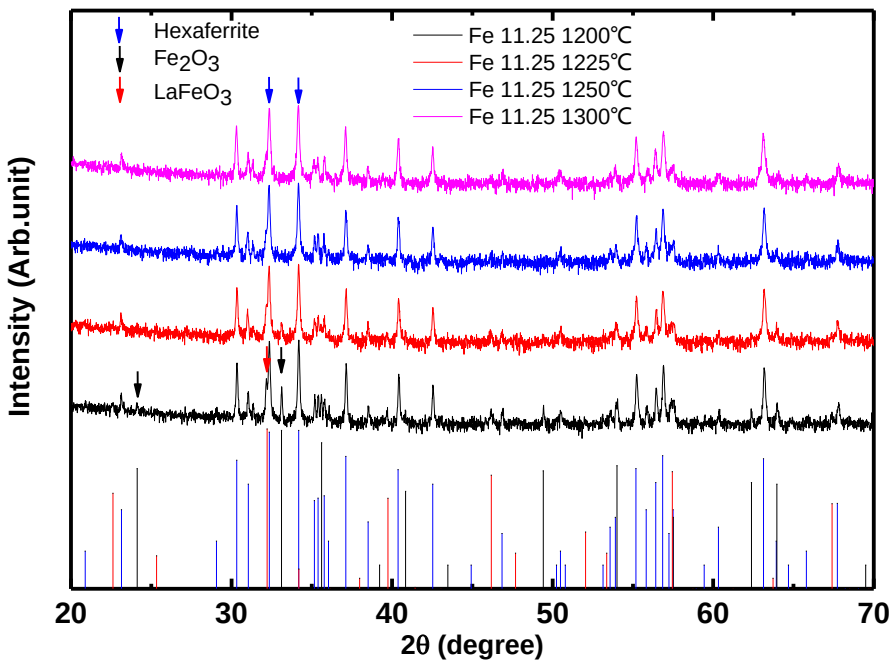

Figure. 4-2(e) XRD patterns of $Sr_{1-x}La_xFe_{11.25}O_{19-\delta}$ calcined in air

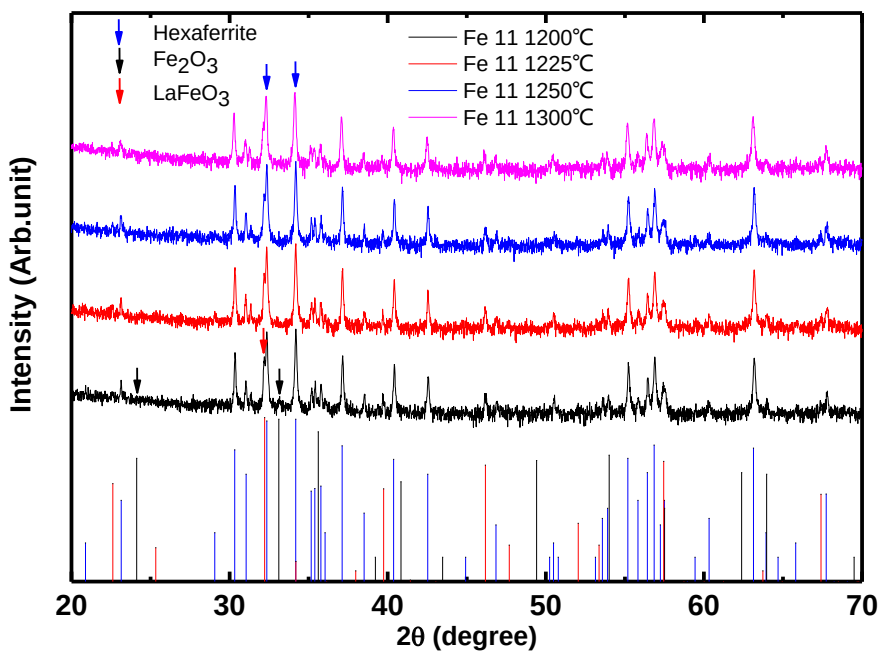

Figure. 4-2(f) XRD patterns of $Sr_{1-x}La_xFe_{11}O_{19-\delta}$ calcined in air

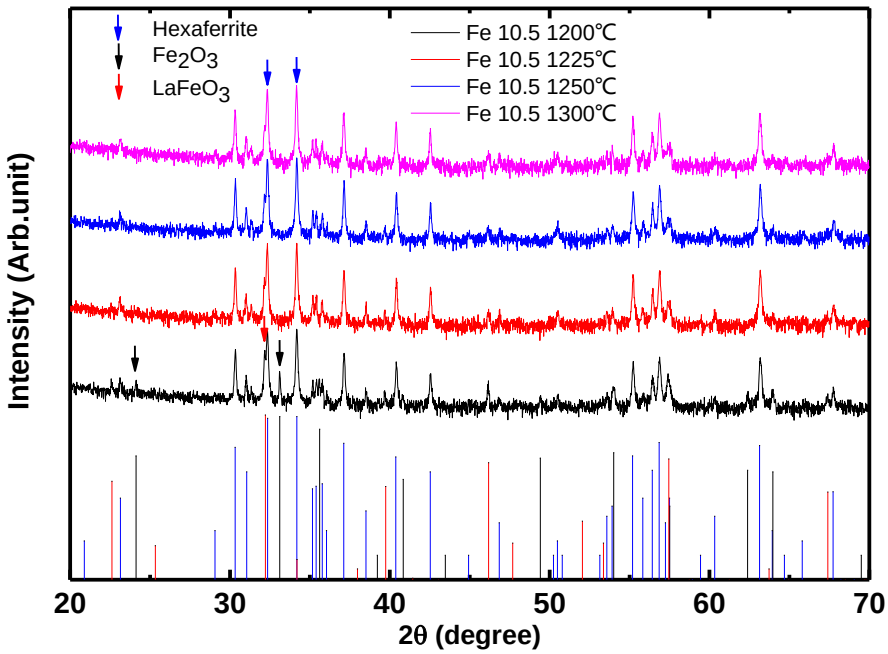

Figure. 4-2(g) XRD patterns of $Sr_{1-x}La_xFe_{10.5}O_{19-\delta}$ calcined in air

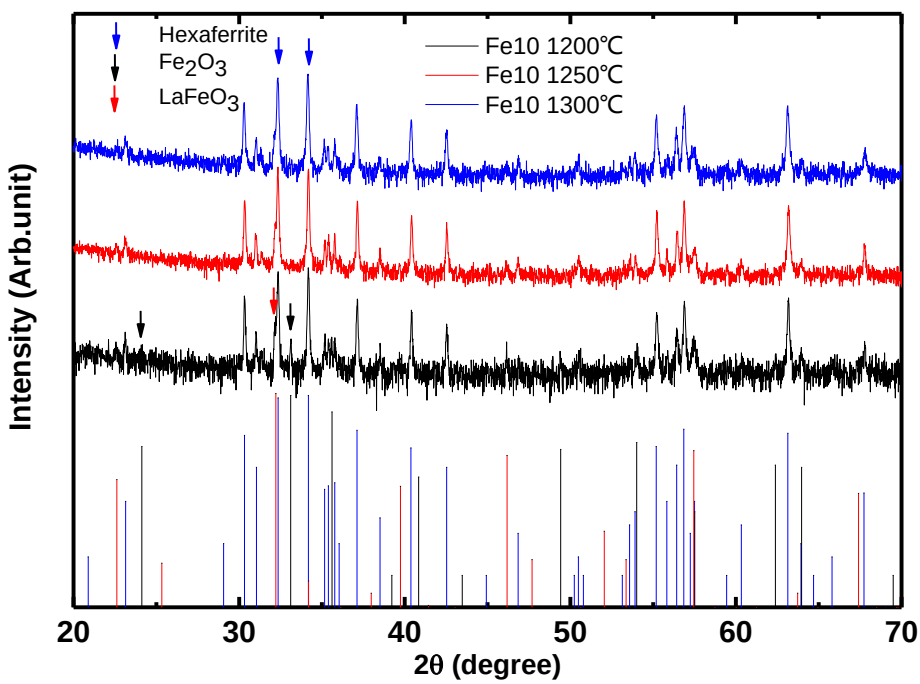

Figure. 4-2(h) XRD patterns of $Sr_{1-x}La_xFe_{10}O_{19-\delta}$ calcined in air

Table. 4-2 Detected phases from XRD patterns of $Sr_{1-x}La_xFe_{12-y}O_{19-\delta}$ after calcination in air

Temperature (°C) / Composition.y	1200	1225	1250	1300
Fe=12.25	M+F+L	M+F+L	M+F	M+F
Fe=12	M+F+L	M+F+L	M	M
Fe=11.75	M+F+L	M+F+L	M	M
Fe=11.5	M+F+L	M+F+L	M	M
Fe=11.25	M+F+L	M+F+L	M+L	M+L
Fe=11	M+L	M+L	M+L	M+L
Fe=10.5	M+F+L	M+L	M+L	M+L
Fe=10	M+F+L	-	M+L	M+L

M: SrM F: Fe_2O_3 L:$LaFeO_3$

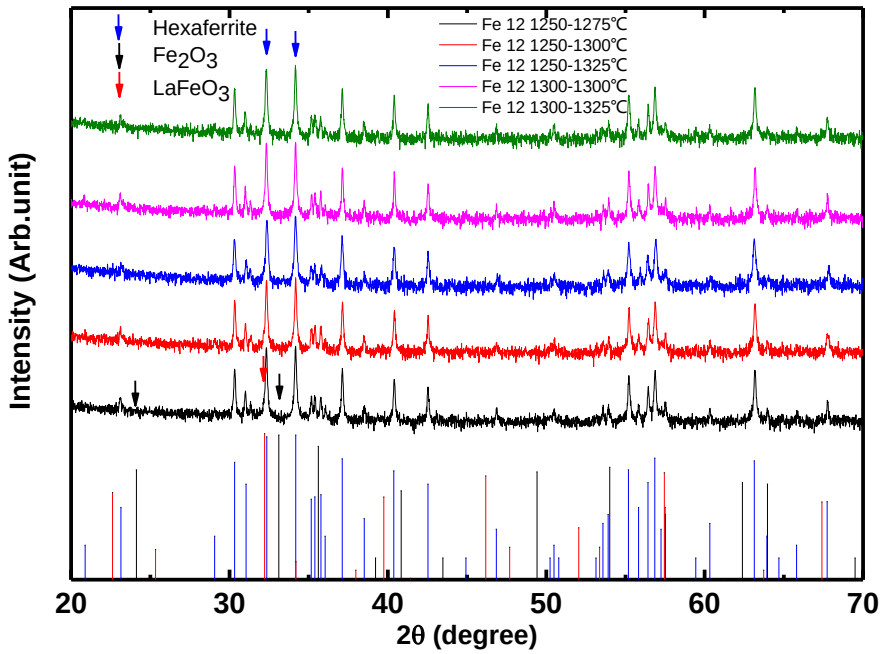

Figure. 4-3(a) XRD patterns of $Sr_{0.5}La_{0.5}Fe_{12}O_{19}$ sintered in air

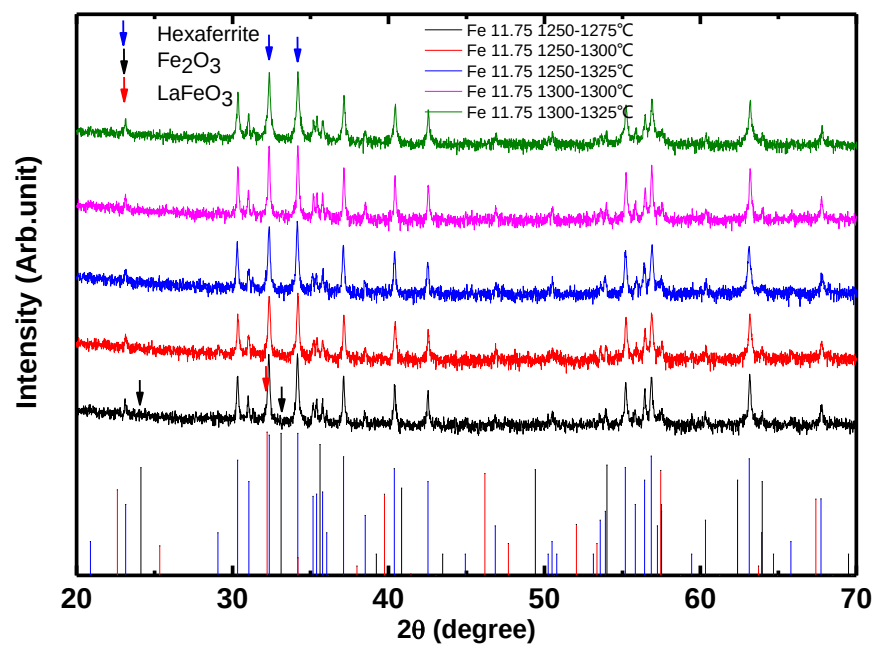

Figure. 4-3(b) XRD patterns of $Sr_{0.5}La_{0.5}Fe_{11.75}O_{19}$ calcined in air

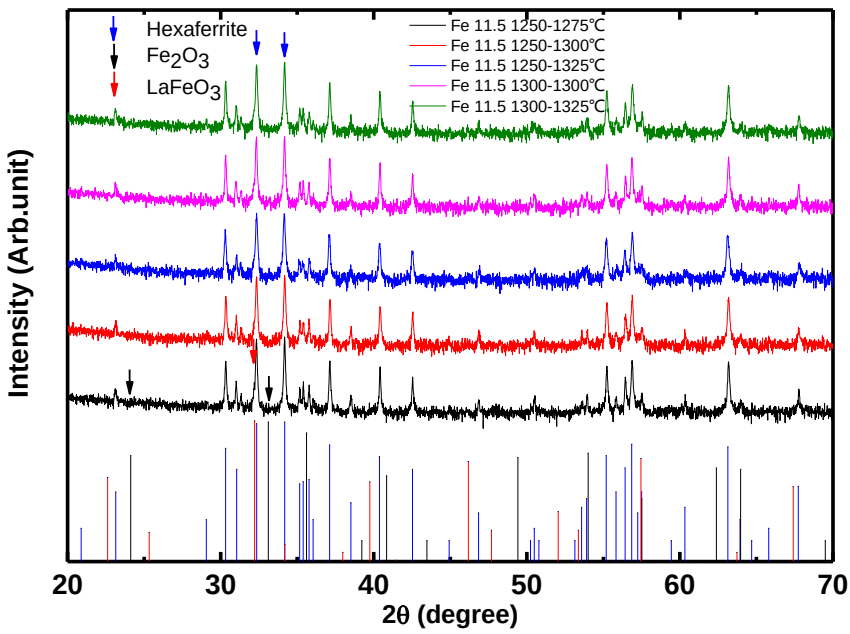

Figure. 4-3(c) XRD patterns of $Sr_{0.5}La_{0.5}Fe_{11.5}O_{19}$ calcined in air.

Table 4-3 Detected phases from XRD patterns of $Sr_{0.5}La_{0.5}Fe_{12-y}O_{19}$ after sintering in air

Temperature (°C) / Composition y	1275	1300	1325
Fe12	M	M	M
Fe11.75	M	M	M
Fe11.5	M	M	M

M: SrM F: Fe_2O_3 L:$LaFeO_3$

4.2 Crystal structure of $Sr_{0.5}La_{0.5}Fe_{12-y}O_{19-\delta}$

The XRD patterns of $Sr_{0.5}La_{0.5}Fe_{12-y}O_{19-\delta}$ ($-0.25 \leqq y \leqq 2$) calcined powder at 1200 - 1300 °C for 8 h to study the effects of iron deficiency was shown in Figures 4-2, which contain the different Fe^{3+}/ Sr^{2+}+La^{3+} ratio, experiment contains samples with ratio value of 12.25,12,11.75,11.5,11.25,11,10.5 and 10. The results were listed in Table 4-2.

Comparing the results listed in Table4-1, 4-2, it was found that single phase M-type hexaferrites $Sr_{0.5}La_{0.5}Fe_{12-y}O_{19-\delta}$ ($0 \leqq y \leqq 0.5$) could be obtained with the decrease in iron content. The sintering process was carried out on these single phase samples and XRD data reviews that all of these samples remains magnetoplumbite structure as in Fig. 4-3 showed, no obvious characteristic diffraction peaks of second phases could be found in the XRD patterns. Fu *et al.* found out that a lower Fe/Sr ratio can improve the magnetic properties and lead to the pure production of pure SrM [23]. But no such large Sr^{2+}/La^{3+} substitution ratio of 1(Sr0.5 and La0.5) have been reported to have single phase hexaferrites structure before.

As shown in Table4-3, the samples were calcined at 1250 °C in air and these calcined samples were sintered at 1275, 1300 and 1325 °C. For the series of samples, the calculated lattice parameters *a*, *c*, and unit cell volume were listed in table 4-5, and 4-6. Lattice parameters *a* and *c* were calculated from the values of d_{hkl} according to the following equation (4-1) [24]:

$$d_{hkl} = \left\{ \frac{4(h^2 + hk + k^2)}{3a^2} + \frac{l^2}{c^2} \right\}^{-1/2} \qquad (4\text{-}1)$$

In which d_{hkl} is the inner-planer spacing, and h, k and l are the Miller indices.

The unit cell volumes were calculated using hexaferrites lattice parameters a and c with the equation (4-2) [25]:

$$V_{cell} = \frac{\sqrt{3}}{2} a^2 \, c \qquad (4\text{-}2)$$

Lattice parameter a did not change much with the iron deficiency, but c was firstly decreased as the content of Fe content declined from 12 to 11.75 ($0 \leqq y \leqq 0.25$), and due to a decline of the content of Fe^{3+} ions, the value of parameter c for all the samples decreased compared with parameter c of pure SrM. From 11.75 to 11.5 ($0.25 \leqq y \leqq 0.5$), a possible reason for increasing of c was attributed to the content of O^{2-} increased, the radius of O^{2-} was larger than Fe^{3+} (O^{2-} = 1.38 Å， Fe^{3+} = 0.55 Å, Fe^{2+} = 0.80 Å, Sr^{2+} = 1.32 Å, La^{3+} = 1.22 Å) [1]. In the other hand, for these single phase samples, the increasing iron deficiency means a higher ratio for Fe^{2+} ions in all Fe ions, and Fe^{2+} ions with a larger ion radius might increase lattice parameter c, due to these factors the lattice parameter c was first decreased and then increased, the Samples as shown in Fig. 4-4(b) were calcined at 1300 °C and sintered at 1300 °C., unit cell volume was decreased initially and then increased substantially with the reduction of Fe content. That could be explained by equation 4-2. For most samples, if we consider lattice parameter a as a constant, than the unit cell volume is in direct proportion to c.

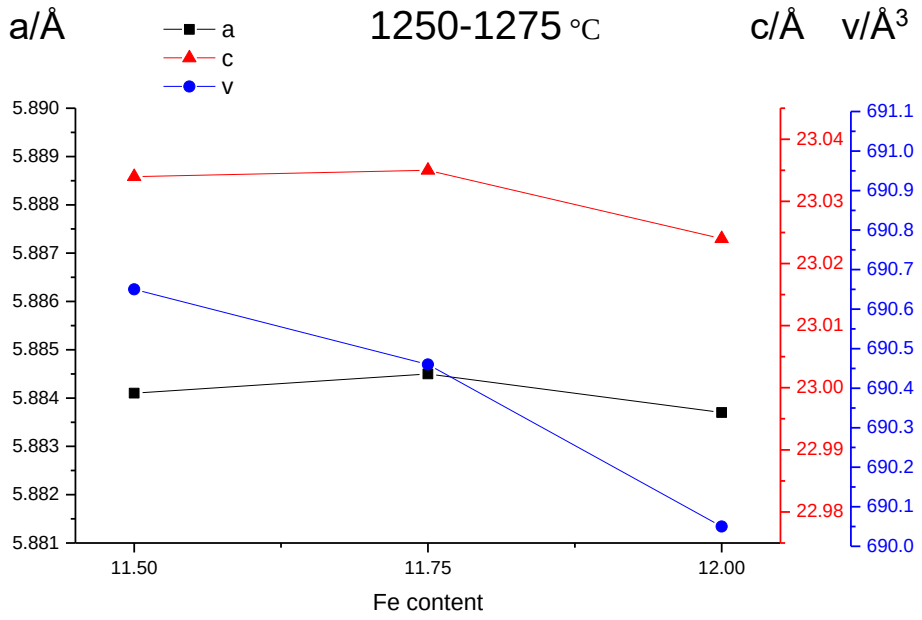

(a) Samples calcined at 1250 °C and then sintered at 1275 °C in air for 8 h, respectively.

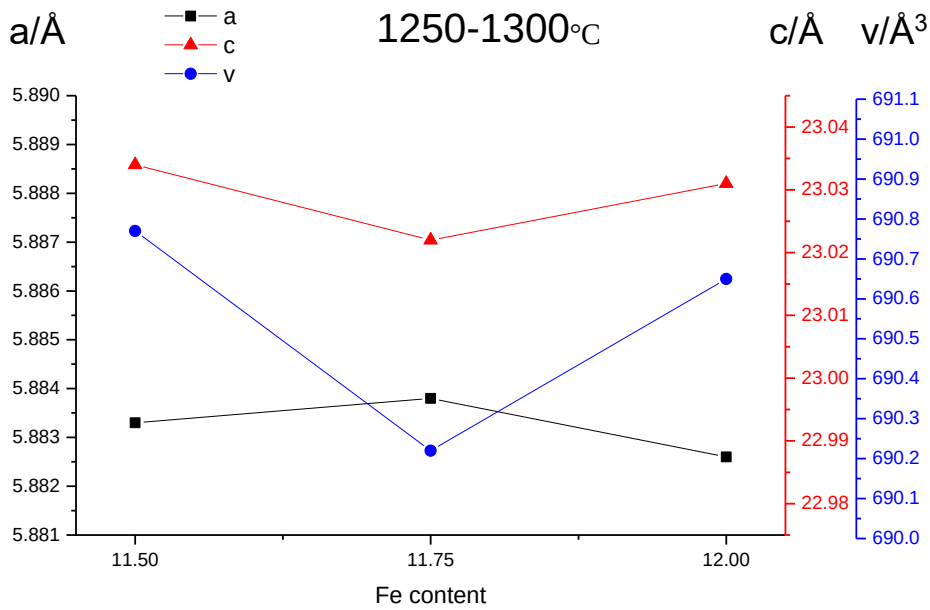

(b) Samples calcined at 1250 °C and then sintered at 1300 °C in air for 8 h, respectively.

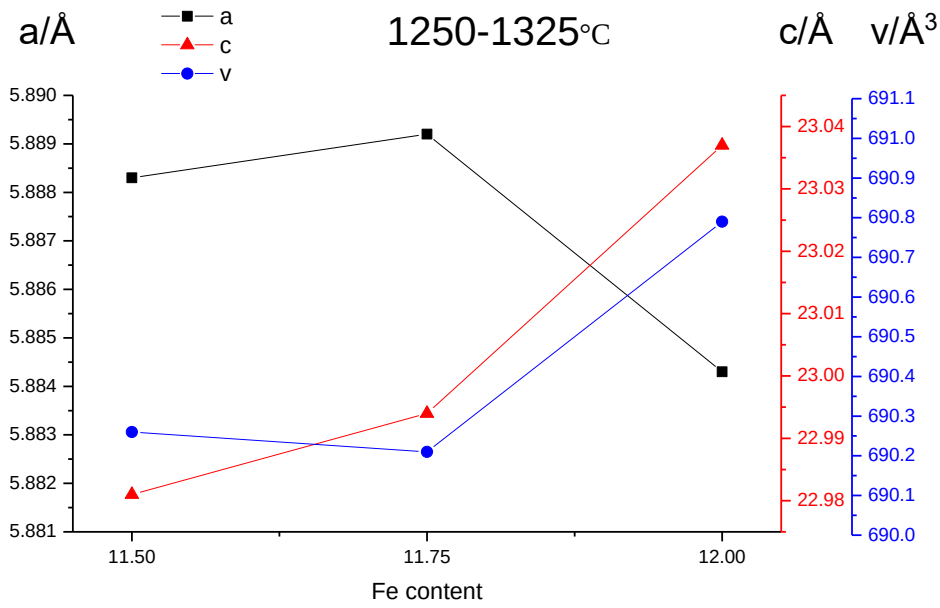

(c) Samples calcined at 1250 °C and then sintered at 1325 °C in air for 8 h, respectively.

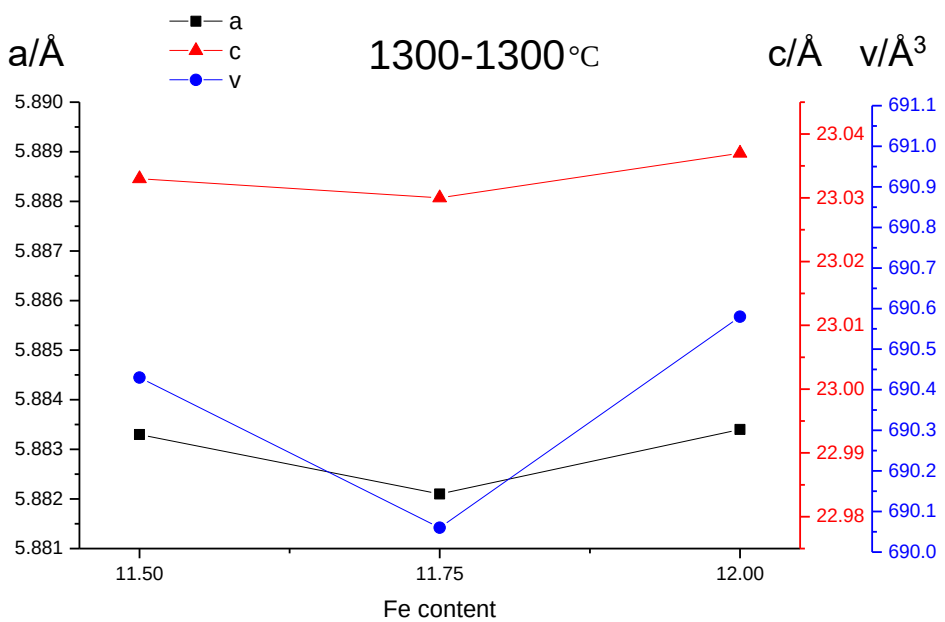

(d) Samples calcined at 1300 °C and then sintered at 1300 °C in air for 8 h, respectively.

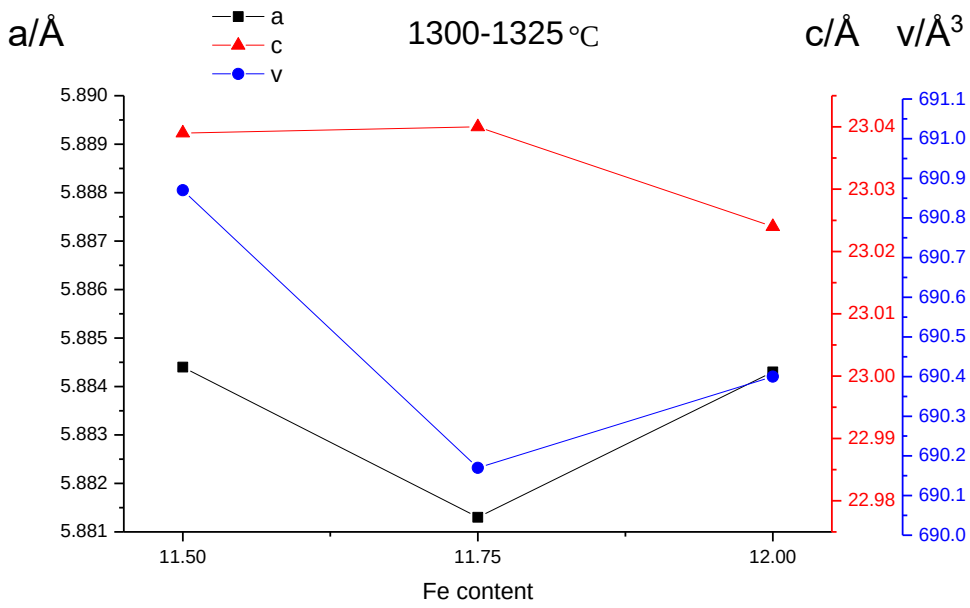

(e) Samples calcined at 1300 °C and then sintered at 1325 °C in air for 8 h, respectively.

Figure4-4. Lattice parameters and unit cell volumes of $Sr_{0.5}La_{0.5}Fe_{12-y}O_{19-\delta}$ samples vs Fe content

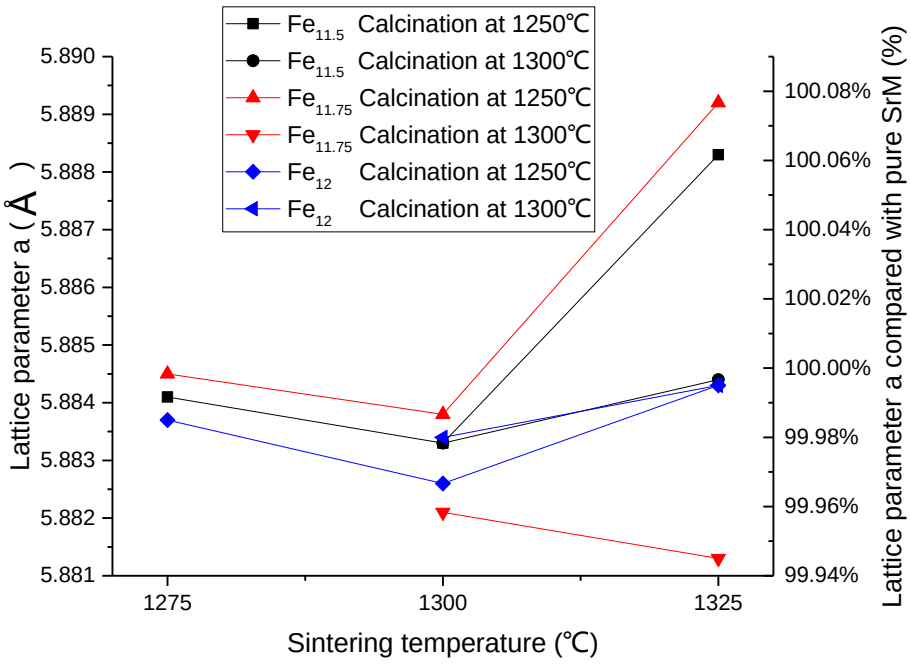

(a) Lattice parameter a of samples sintered at 1275, 1300, and 1325 °C.

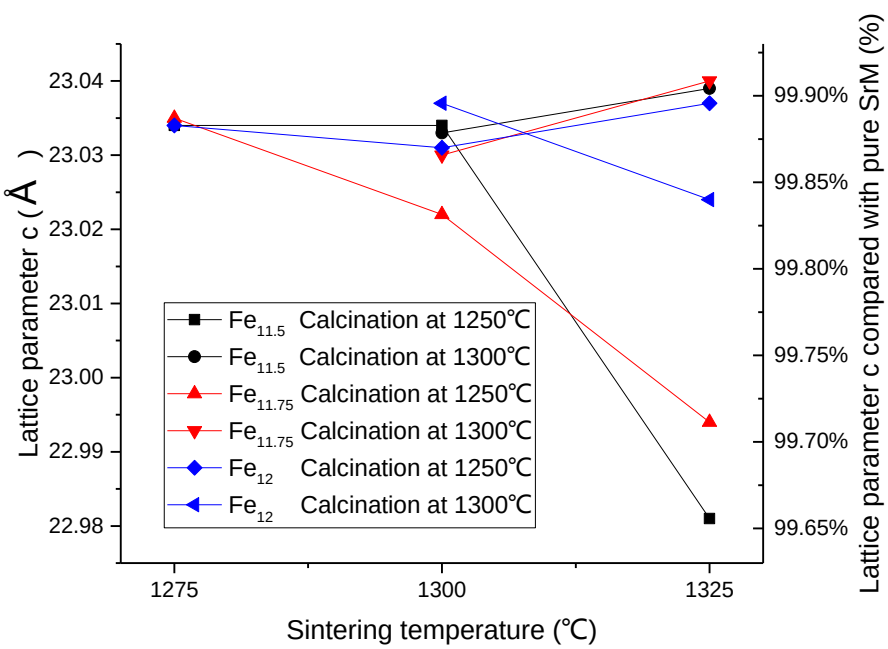

(b) Lattice parameter c of samples sintered at 1275, 1300, and 1325 °C.

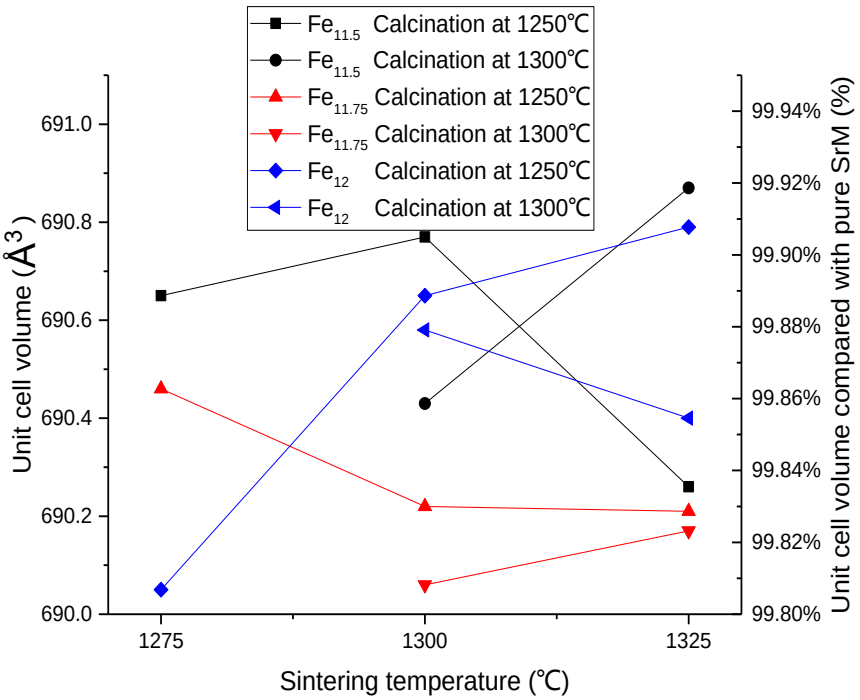

(c) Unit cell volumes of samples sintered at 1275, 1300, and 1325 °C.

Figure4-5. Lattice parameters and unit cell volumes of $Sr_{0.5}La_{0.5}Fe_{12-y}O_{19-\delta}$ samples when sintered at 1275, 1300, and 1325 °C.

Figure 4-5 showed the lattice parameters and unit cell volumes of $Sr_{0.5}La_{0.5}Fe_{12-y}O_{19-\delta}$ samples when sintered at 1275, 1300, and 1325 °C.Maximum change rate in lattice parameter a was 0.12%, while in c was 0.3%, and in unit cell volume was 0.12%, in that case we can consider change in c in the main factor of unit cell shrinking.

At 1300°C the sample with Fe content of 11.75 has the lowest lattice parameter c and unit cell volume values.

Table 4-4. Sintered density and relative density of

$Sr_{0.5}La_{0.5}Fe_{12-y}O_{19-\delta}$ samples ($0 \leqq y \leqq 0.5$)

Calcination-Sintering temperature (° C)	Fe content (y)	Sintered Density (g/cm^3)	Relative density (%)
1250-1275	11.5	4.80(2)	94.1
	11.75	4.82(3)	93.2
	12	4.86(6)	91.3
1250-1300	11.5	4.80(3)	94.1
	11.75	4.86(3)	94.0
	12	4.92(5)	90.9
1250-1325	11.5	4.82(2)	94.5
	11.75	4.90(3)	94.7
	12	4.96(4)	94.0
1300-1300	11.5	4.81(5)	94.3
	11.75	4.92(4)	95.1
	12	4.97(6)	95.0
1300-1325	11.5	4.85(4)	95.0
	11.75	4.99(1)	96.5
	12	4.99(2)	95.4

The theoretical density ρ_{th}=5.23g/cm^3 for y = 0, 5.17g/cm^3 for y =0.25, and 5.10g/cm^3 for y =0.5, respectively, calculated by equation 3-2.

Table 4-5 Lattice parameters and unit cell volumes for $Sr_{0.5}La_{0.5}Fe_{12-y}O_{19-\delta}$ samples, which were calcined at 1250 °C for 8 h in air, and then sintered at 1275, 1300, and 1325 °C for 2 h in air.

La ratio	Fe content	Sintering Temp(℃)	a (Å)	c (Å)	c/a	Unit Cell Volume/Å^3
0.5	11. 5	1275	5.8841	23.034	3.9146	690.653
	11.75		5.8845	23.035	3.9145	690.777
	12		5.8837	23.024	3.9131	690.259
	11. 5	1300	5.8833	23.034	3.9151	690.465
	11.75		5.8838	23.022	3.9127	690.223
	12		5.8826	23.031	3.9151	691.211
	11.5	1325	5.8883	22.981	3.9028	690.048
	11.75		5.8892	22.994	3.9044	690.649
	12		5.8843	23.037	3.9149	690.790

Table 4-6 Lattice parameters and unit cell volumes for $Sr_{0.5}La_{0.5}Fe_{12-y}O_{19-\delta}$ samples, which were calcined at 1250 °C for 8 h in air, and then sintered at 1275, 1300, and 1325 °C for 2 h in air.

La ratio	Fe content	Sintering Temp(℃)	a (Å)	c (Å)	c/a	Unit Cell Volume/Å^3
0.5	11. 5	1300	5.8833	23.033	3.9149	690.435
	11.75		5.8821	23.030	3.9152	690.064
	12		5.8834	23.037	3.9155	690.578
	11.5	1325	5.8844	23.039	3.9152	690.873
	11.75		5.8813	23.040	3.9175	690.175
	12		5.8843	23.024	3.9127	690.400

4.3 Microstructure and morphology of $Sr_{0.5}La_{0.5}Fe_{12-y}O_{19-\delta}$.

SEM micrographs of samples with different Fe content (y) of 0, 0.25, 0.5, were shown in Fig. 4-6. As shown in this figure, it is observed that the hexaferrite magnets are formed of hexagonal-shaped crystals, and the phases were perfect crystalline hexaferrites. The average grain sizes were measured from the SEM micrographs using an image-analyzing software (Image-Pro Plus) [26]. The average grain size was about 2 μm, which reduced with y increasing. The grain size distribution was shown in Fig. 4-7.

As Fe content decreased, iron vacancy and oxygen vacancy of crystal structure existed were increased, which could induce to an increase of grain size.

In the sample micrographs, we could clear see the imperfect domain boundary indicated that these samples are not single domain samples, which can get the best magnetic properties [6].

It could be because of the limit of ceramic method. It was reported that the theoretical limit of grain size was 0.9 μm and the experimental limit of grain size was 1.3 μm [6]. A proper ball-milling time might be essential to improve the powder quality.

(a)

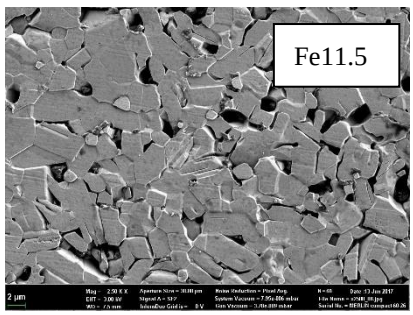

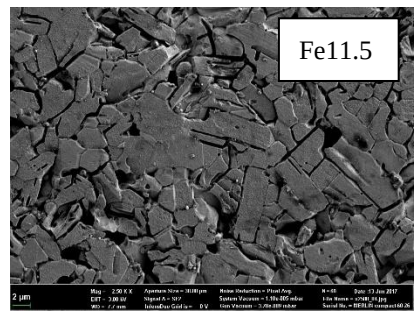

(b)

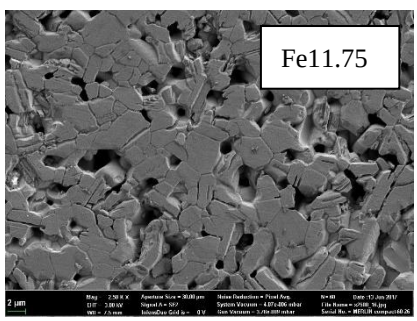

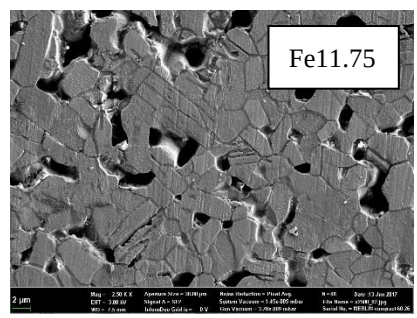

(c)

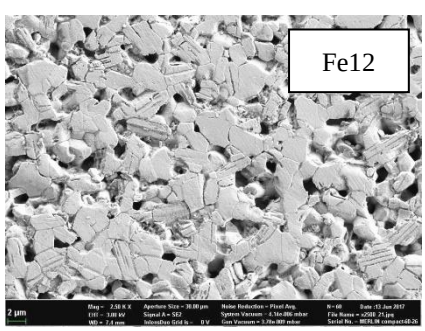

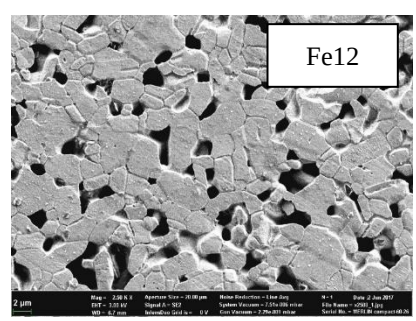

Figure 4-6. SEM image of $Sr_{0.5}La_{0.5}Fe_xO_{19-\delta}$, sintered at 1300 & 1325 °C in air for 2 h

Table 4-7 Grain size distribution of $Sr_{0.5}La_{0.5}Fe_{12-y}O_{19-\delta}$ compositions sintered at 1300 °C for 2 h after calcination at 1300 °C for 8 h in air

Fe content (12y)	Ave. Grain Size (μm)	
11.5	1.58	2.23
11.75	1.72	2.39
12	1.88	2.35

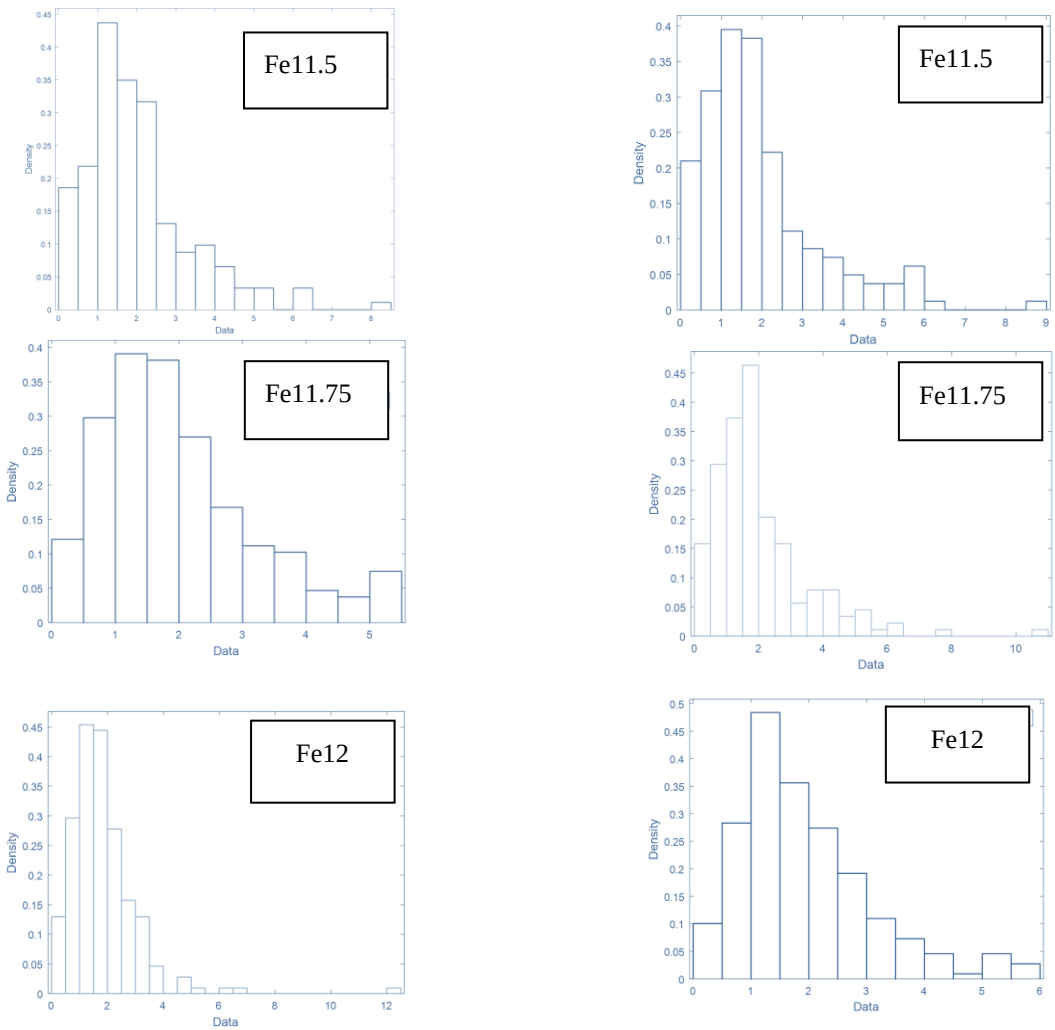

Figure 4-7 Average grain size distribution of $Sr_{0.5}La_{0.5}Fe_{12-y}O_{19-\delta}$ samples sintered at 1300 °C for 2 h after calcination at (a)1250 °C (b)1300 °C for 8 h.

4.4 Magnetic properties of $Sr_{0.5}La_{0.5}Fe_{12-y}O_{19-\delta}$

Hysteresis loops of $Sr_{0.5}La_{0.5}Fe_{12-y}O_{19-\delta}$ are shown in Fig. 4-8. The magnetization datum were fitted by applying the law of approach to saturation, as equation (4-3) [26,27].

$$M = M_S(1 - A/H - B/H^2) + \chi_P H \qquad (4\text{-}3)$$

In which M_s is the saturation magnetization. The term described the field-induced increase in the spontaneous magnetization of the domains, or forced magnetization; this term is usually small at temperatures well below the Curie point and may often be neglected. Constant A is generally interpreted as due to inclusions and microstress, and constant B is proportional to K^2 (K is the anisotropy constant). And in a strong magnetic field case, the term *A/H* could be neglected too. Thus, the equation (4-3) can be simplified as (4-4) [28].

$$M = M_S(1 - B/H^2) \qquad (4\text{-}4)$$

Therefore, in a high applied magnetic field, M-H curves are fitted with equation (4-4), the values of saturation magnetization M_s could be calculated.

Positive value and negative value of the H_c and M_r could be read from the hysteresis loops correspondingly, the average value between them are the H_c and M_r values. From the Table.4-8, M_s is changing with y increasing, but not significantly. M_s is slightly modified in all samples since its value depend on composition, crystallinity and the presence of non-magnetic phases as hematite. Liu *et al*. [1] have the viewpoint that superexchange interactions determine the

orientation of magnetic moment of Fe^{3+} ions, and their $Sr_{0.5}La_{0.5}Fe_{12}O_{19-\delta}$ sample showed a M_s of 55 emu/g when sintered at 1300 °C. The lowest saturation magnetization value of 67.4 emu/g was obtainable for the $Sr_{0.5}La_{0.5}Fe_{11.75}O_{19-\delta}$ sample which was calcined at 1300 °C for 8 h in air prepared at y is 0.25 and sintered at 1325 °C for 2 h in air; The maximum M_s was 72.8 emu/g sintered at 1325 °C for 2 h in air, when y is 0.5.

The balance of saturation magnetization has two factors. The first factor is that La^{3+} substituted Sr^{2+} in SrM ferrites and which lead to Fe^{3+} ions have a valence change to Fe^{2+}. the increasing iron deficiency increased the solubility of La^{3+} caused the number of Fe^{3+} at preferential 2a and 4f2 sites increased and there were more Fe^{2+} with less Bohr magneton number, lead to an increase in net magnetic moment, thus enhanced the saturation magnetization.

The second factor of iron deficiency to saturation magnetization are the increasing iron deficiency decreased the amounting number of iron ions with spin up orientation and weaken the superexchange interaction, also the iron deficiency lead to higher La^{3+} to Fe^{3+} ratio and weaken the so called canting spin structure, which lead to a decrease in the saturation magnetization. The two factors effects on the M_s together so that it showed a constantly changing in all tested samples.

Though the comparison table 4-9, we can see the value of M_s of Sr-La-Co M-type hexaferrites were slightly larger than that of the pure Sr or Ba M-type hexaferrites without substitution. And for the Ba-Ir-Co-Bi M type hexaferrites, due to the substitution of Ir and Bi, the higher M_s=86 emu/g was obtained [34]. In my study, the M_s = 72.8 emu/g of composition $Sr_{0.5}La_{0.5}Fe_{11.5}O_{19-\delta}$ without Co

substitution, but less content of Fe than stoichiometry was obtained. The magnetic properties are the same level with the previous reports [1-4].

Z.Y.Wang *et al*, have studied the effect of temperature on coercivity ($\boldsymbol{H_c}$)and suggested that with an increasing temperature more than 1280 °C the grain sizes of SrM ferrites grow and grain became coarse, which could explain the decreasing of coercivity compared to the pure SrM. [25]

The possible reason for low H_c could be the decreasing intrinsic coercivity when temperature raised that magnetic alignment became harder and particles grown. Because the amount of Fe^{3+} decreased, it makes the Fe-O super exchange interaction proportionally weak, resulting in decreased M_s.

There is a close relation between H_c and grain size. Based on the previous SEM investigations, it has been shown that an increase is observed before the decline in grain size. Thus, H_c shows a decrease before an increase in grain size (Table 4.7).

As reported in the research [29]，the authors suggested that a lower Fe^{3+}/Sr^{2+} mole ratio than stoichiometry leads to the production of iron and oxygen vacancies，a phenomenon which is similar to the present experiment where the lower Fe^{3+}/Sr^{2+} or La^{3+} enhances the ionic diffusion and improve the magnetic properties. However, the images taken by SEM showed the average grain size is larger than the size of single domain; it could result in the small value of H_c.

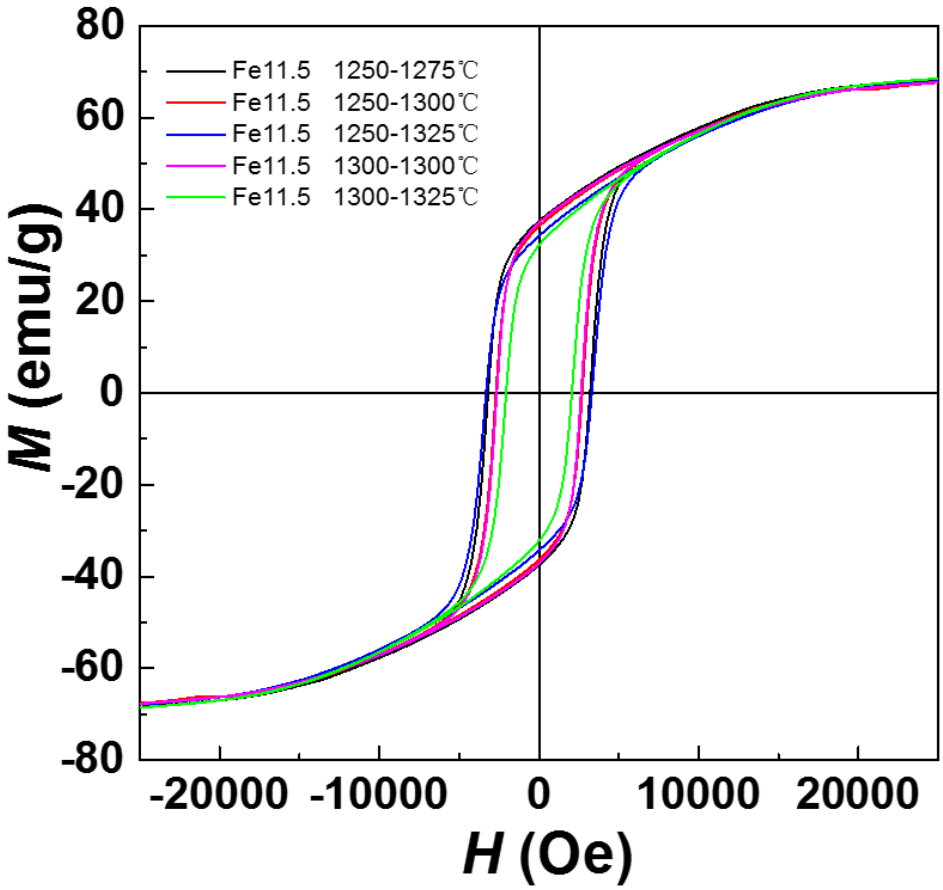

(a) Hysteresis loops for $Sr_{0.5}La_{0.5}Fe_{11.5}O_{19-\delta}$ sintered for 2 h in air.

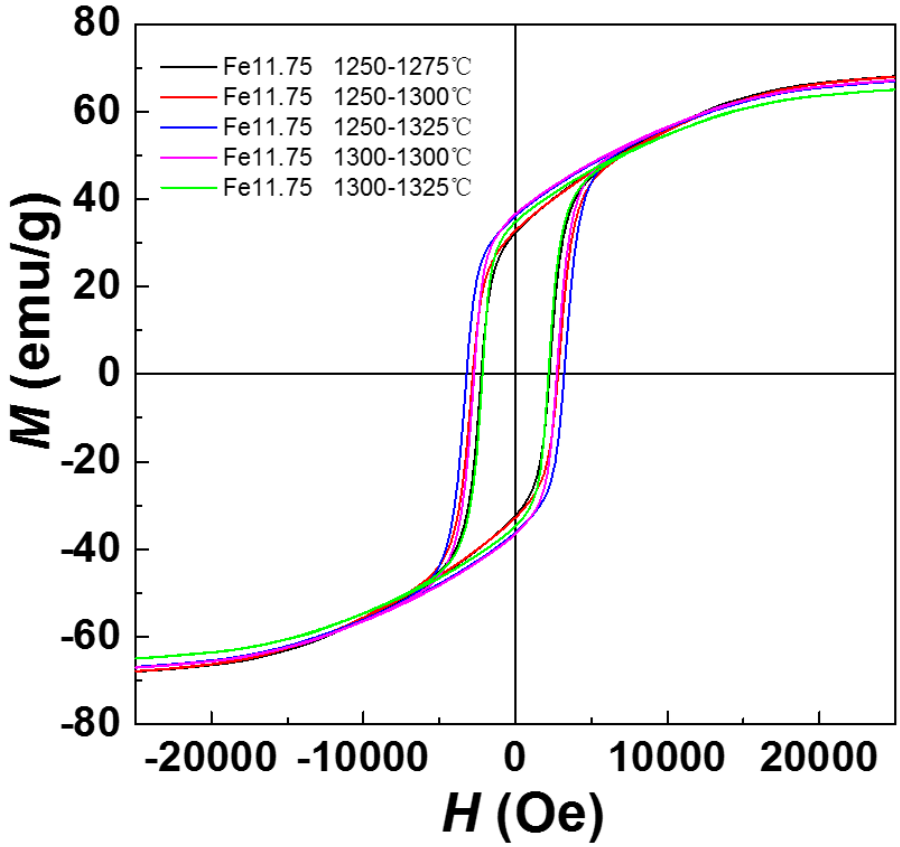

(b) Hysteresis loops for $Sr_{0.5}La_{0.5}Fe_{11.75}O_{19-\delta}$ sintered for 2 h in air.

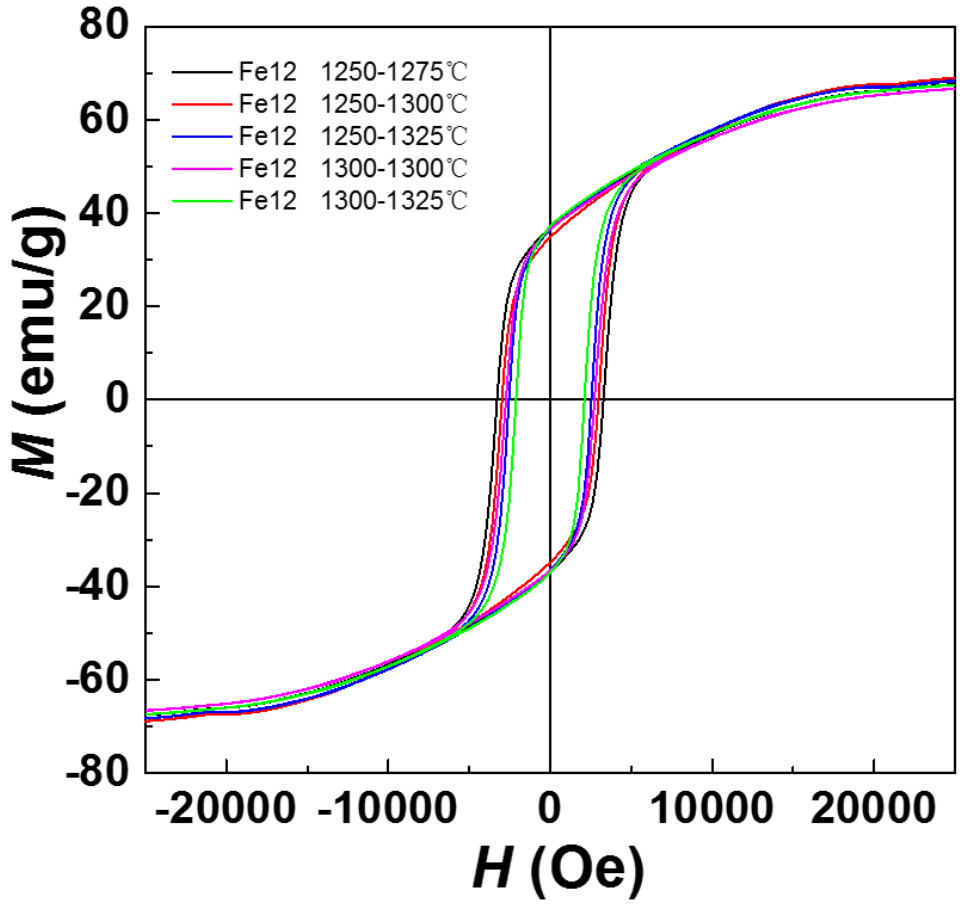

(c) Hysteresis loops for $Sr_{0.5}La_{0.5}Fe_{12}O_{19-\delta}$ sintered for 2 h in air.

Figure4-8. Hysteresis loops of $Sr_{0.5}La_{0.5}Fe_{12-y}O_{19-\delta}$ samples vs Fe content

Table 4-8 Magnetic properties of $Sr_{0.5}La_{0.5}Fe_{12-y}O_{19-\delta}$ ($0 \leqq y \leqq 0.5$) sintered in air

Fe ratio #	Calcination & Sintering temperature (°C)	M_s (emu/g)	M_r (emu/g)	H_c (Oe)	$(BH)_{Max}$ (MGOe)
11.5	1250-1275	70.9	37	3194	3.79
11.75		70.7	32	2238	2.16
12		69.9	36	3282	3.8
11.5	1250-1300	69.6	36	2701	3.7
11.75		70.8	32	2807	2.8
12		71	35	2976	3.38
11.5	1250-1325	72.8	35.1	3300	3.58
11.75		69.5	35	3300	3.7
12		70.1	36	2545	3.08
11.5	1300-1300	70.2	37	2639	3.21
11.75		69.6	36	2716	3.2
12		69.2	36	2729	3.3
11.5	1300-1325	71.4	32	2058	1.93
11.75		67.4	34	2172	2.45
12		69.9	37	2113	2.57

Yang *et al.* [30] reported with La-Co substitution, Sr-Ca hexaferrites could be synthesized with $(BH)_{max}$ of 4.3 MGOe, Pure SrM have a $(BH)_{max}$ of 3.6 MGOe [6].

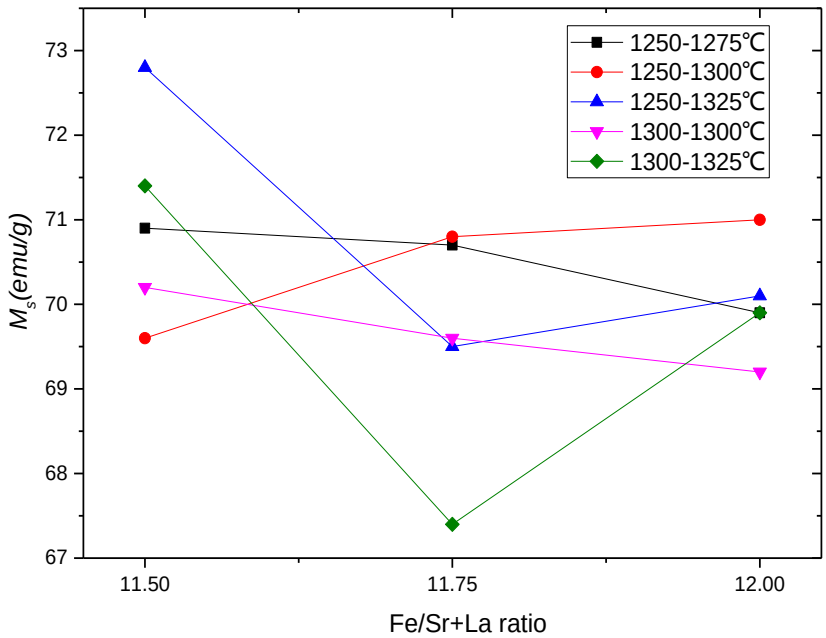

Figure. 4-9 Saturation magnetization Vs Fe content

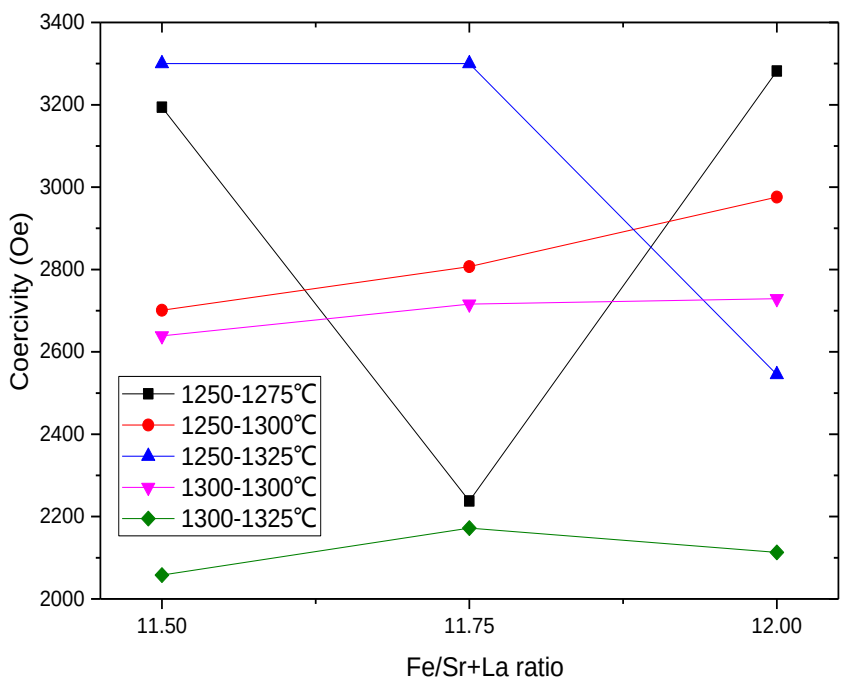

Figure. 4-10 Coercivity Vs Fe content

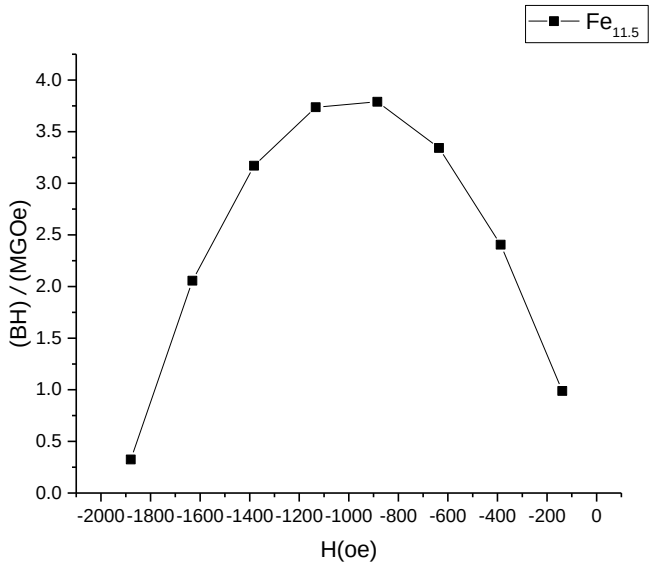

(a) BH-H curve of $Sr_{0.5}La_{0.5}Fe_{11.5}O_{19-\delta}$ samples, with (BH)max value of 3.79 MGOe at H= -884.8 Oe

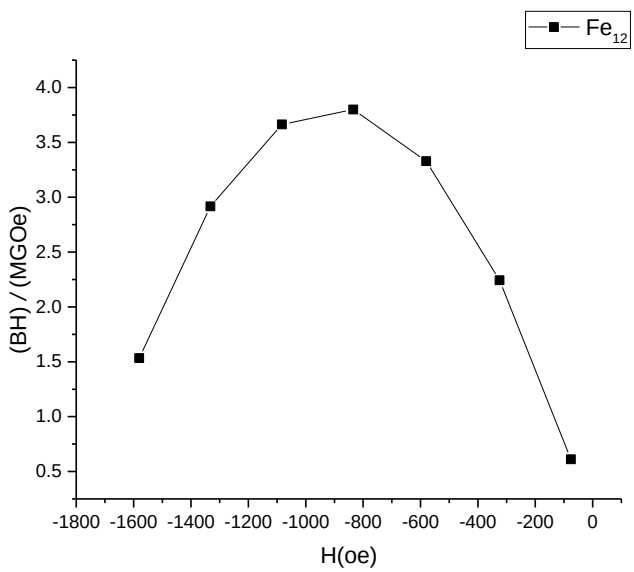

(b) BH-H curve of $Sr_{0.5}La_{0.5}Fe_{12}O_{19-\delta}$ samples, with (BH)max value of 3.8 MGOe at H= -834.3 Oe

Figure. 4-10 BH-H curve of $Sr_{0.5}La_{0.5}Fe_{12-y}O_{19-\delta}$ samples, calcination at 1250°C for 8 h, and then sintered at 1275 °C for 2 h.

Table. 4-9 Comparison of saturation magnetization of M-type hexaferrites

Composition	M_s (emu/g)	Reference
$SrFe_{12}O_{19}$	Up to 70	[31]
$BaFe_{12}O_{19}$	68	[32]
$Sr_{0.65-x}Sr_xLa_{0.35}Fe_{11.32}Co_{0.28}O_{18.435}$	75.3(x=0.2)	[33]
$BaFe_{10.25}Ir_{0.85}Co_{0.85}Bi_{0.05}O_{19}$	86	[34]
$Sr_{0.5}La_{0.5}Fe_{10.25}O_{19-\delta}$	72.8	Present study
$Sr_{0.5}La_{0.5}Fe_{11.25}O_{19-\delta}$	71.4	Present study

5. Conclusion

In this study, $Sr_{1-x}La_xFe_{12}O_{19}$ and $Sr_{0.5}La_{0.5}Fe_{12-y}O_{19-\delta}$ were synthesized by conventional ceramic reaction. The effect of iron deficiency on micro structure and magnetic properties of $Sr_{0.5}La_{0.5}Fe_{12-y}O_{19-\delta}$ were investigated.

Firstly, M-type Hexaferrites $Sr_{0.5}La_{0.5}Fe_{12-y}O_{19-\delta}$ samples were calcined at 1250 and 1300 °C for 8 h in air, which having the solubility limit of $0 \leq y \leq 0.5$, single phase hexaferrites was obtainable. It has never been reported yet on Sr-La M-type single phase hexaferrites with Sr/Fe ion ratio of 0.5/0.5. So that iron deficiency could be a beneficial factor for synthesis of single phase Sr-La M-type hexagonal ferrites just like the Sr-La-Co M-type ferrites.

Secondly, for the single phase $Sr_{0.5}La_{0.5}Fe_{12-y}O_{19-\delta}$ ferrites sintered at 1300 °C for 2 h in air, the lattice parameters *a*, *c* and the unit cell volume were all decreased initially but increased later with increasing y. It was revealed from SEM investigations that the average grain size of the sample with the same sintering condition was about 2 μm and it shows a decreasing tendency with iron deficiency when sintered at 1300 °C for 2 h. Also, as y increased, the saturation magnetization M_s is about 70 emu/g, but H_c decreased compare to the previous report, which could be a defect effect of high temperature. Iron deficiency can lead to the production of iron and oxygen vacancies, which could enhance the diffusion among various ions. Thus, the magnetic properties could be improved. The magnetic properties of Sr-La slightly increased with iron deficiency, the optimal M_s of 72.8 emu/g was obtainable with a coercivity of 3300 Oe for this $Sr_{0.5}La_{0.5}Fe_{12-y}O_{19-\delta}$ sample sintered at 1325˚C for 2 h in air.

The maximum energy product was 3.8 MGOe for $Sr_{0.5}La_{0.5}Fe_{12}O_{19-\delta}$ samples sintered at 1275 ˚C for 2 h and 3.79 MGOe for $Sr_{0.5}La_{0.5}Fe_{11.5}O_{19-\delta}$ sintered at 1275 ˚C for 2 h. The properties of ferrites synthesized implying that it must be a promising alternative to current M-type hexaferrites for permanent magnet applications.

References

[1] Liu X S, Zhong W, Gu B X et al, *Rare Metal Materials and Engineering*, 31-5: 385 (2002)

[2] Hu, Feng, et al, *Journal of Applied Physics* 109.11 (2011): 113906.

[3] Wang, J. F., et al. *Journal of alloys and compounds* 369.1 (2004): 170-177.

[4] Chen, Deyang et al, *Materials Research Express* 3.4 (2016): 045002.

[5] Liu, Xian song, et al., *physica status solidi* (a) 193.2 (2002): 314-319.

[6] Pullar, Robert C. *Progress in Materials Science* 57.7 (2012): 1191-1334.

[7] Coey J M D, Magnetic materials[J]. *J Alloys and Compounds*,2001,326(1):2-6.

[8] Figure from *Journal TDK*, 17(2017)

[9] Y.F. Wang, Q.L. Li, C.R. Zhang, B.D. Li, *J. Magn. Mater.* 321 (2009) 3368–3372

[10] Sudakar C, Subbanna GN, Kutty TRN. *J Magn Magn Mater* 2003; 263:253.

[11] R. Müller, R. Hiergeist, W. Gawalek, A. Hoell, A. Wiedenmann, *Journal of Magnetism and Magnetic Materials*, 252, 43-45(2002)

[12] R. Murakami, K. Shima, H. Kakuta, H. Takamura, T. Tanaka, M. Okada, M.Fukuda, M. Sano, K. Kamino, *Materials Transactions*, 37, 499-502(1996)

[13] Seifert, D., et al. *Journal of Magnetism and Magnetic Materials* 321.24 (2009): 4045-4051.

[14] Lei, Chenglong, Shaolong Tang, and Youwei Du. *Ceramics International* 42.14 (2016): 15511-15516.

[15] Lechevallier, L., et al. *Journal of magnetism and magnetic materials* 269.2 (2004): 192-196.

[16] Z.W.Li, L.Chen, C.K.Ong, *Journal of Applied Physics*, 923902-3907(2002)

[17] T. Zemcik, Fresenius I, *Journal of Analytical Chemistry*, 349 26-31(1994)

[18] Kools F., Morel A., Grössinger R., et al. *Journal f magnetism and magnetic materials*, 2002, 242: 1270-1276.

[19] Tenaud P., Morel A., Kools F., et al. *Journal of alloys and compounds*, 2004, 370(1): 331-334.

[20] Lechevallier L., Le Breton J.M., Teillet J., et al. *Physica B: Condensed Matter*, 2003, 327(2): 135-139.

[21] Lechevallier L., Le Breton J.M., Morel A, et al. *Journal of alloys and*

compounds, 2003, 359(1): 310-314.

[22] Wang, Zhanyong, et al. *Journal of Superconductivity & Novel Magnetism* 26.12 (2013).

[23] Fu, Yen-Pei, and Cheng-Hsiung Lin. *Journal of Alloys and Compounds* 386.1 (2005): 222-227.

[24] Y.M Kang, Y.H Kwon, M.H Kim, D.Y Lee, *Journal of Magnetism and Magnetic Materials*, 382, 10-14(2015)

[25] Li, Wangchang, et al. *Materials Research Bulletin* 48.11 (2013): 4449-4453.

[26] A. Kihal, G. Fillion, B. Bouzabata, B. Barbara, *Physica Status Solidi*, 249, 604-614(2012)

[27] S. Ounnunkad, P. Winotai, *Journal of Magnetism and Magnetic Materials*, 301, 292–300(2006)

[28] B.G. Toksha*, Solid State Communications*, 147, 479–483(2008)

[29] F.L Zan, Y.Q Ma, X Zhang, Q Ma, G.H Zheng, Z.X Dai, *Journal of Anhui University*, 38, 45-54(2014)

[30] Yang, Yujie, et al. *Materials Research Bulletin* 59 (2014): 37-41.

[31] H.Sözeri, A.Baykal, B. Ünal, *physica status solidi*, 209, 2002-2013 (2012)

[32] Kojima H, *Ferromagnetic materials*, 3, 658-659 (1982)

[33] Y.J Yang, X.S Liu, *Transactions on magnetics*, 50, 234-236(2013)

[34] B. Sugg, H. Vincent, *Journal of Magnetism and Magnetic Materials*, 139, 364-370(1995)

초록

SrM 헥사페라이트에 관한 연구를 진행 하면서, $SrFe_{12}O_{19}$ 은 많은 연구 그리고 업체의 이슈로 되였고 낮은 제조 원가, 부식에 견디는 능력, 그리고 높은 자성 특성을 가지고 있습니다. 이번 연구는 우선 $Sr_{0.5}La_{0.5}Fe_{12-y}O_{19-\delta}$ 을 합성하였고, 싱글 헥사페라이트를 다음과 같이 $0 \leqq y \leqq 0.5$ 으로 지정하였고, 철이 결정구조에 들어가는 정도 그리고 헥사페라이트의 자성 물성에 대해서 연구하였습니다.

Sr-La M-type 인 헥사페라이트는 다음과 같이 $Sr_{1-x}La_xFe_{12}O_{19}$(x=0.4, 0.5 and 0.6) 과 $Sr_{0.5}La_{0.5}Fe_{12-y}O_{19-\delta}$ ($-0.25 \leqq y \leqq 2$) 두가지 물질을 고체반응으로 합성하였고, 모든 파우더는 La_2O_3, $SrCO_3$, 그리고 Fe_2O_3 은 순도가 99.9%을 넘습니다. 파우더 무게를 측정하고, 24 시간 볼 밀링 하였고, 펠렛에 다시 넣었습니다. 만들어진 펠렛을 온도가 1150, 1200, 1225, 1250, 그리고 1300° C 에서 에어조건으로 8 시간 진행을 하였고, 최종 M-type 헥사페라이트가 만들어졌습니다. 칼시나이션으로 반복적인 제조를 하였고, 만들어진 펠렛을 다시 1275, 1300 그리고 1325° C 에서 2 시간동안 방치하였습니다. 만들어진 샘플을 XRD 를 통하여 결정구조를 확인 하였고, FE-SEM 으로 마이크로 구조를 확인하였습니다. 자성 물성은 VSM 을 통하여 확인하였습니다.

XRD 패턴으로 Sr-La M-type 인 헥사페라이트 $Sr_{0.5}La_{0.5}Fe_{12-y}O_{19-\delta}$ 는 합당한 피크를 보였고 y($0 \leqq y \leqq 0.5$) 그리고 온도가 1250 이랑 1300° C 에서 8 시간 방치한 샘플이 가장 좋은 성능을 보임을 증명하였습니다. 2 시간동안 방치한 샘플은 분해가 되지는 않았지만

싱글형상을 유지하고 있었습니다. $Sr_{0.5}La_{0.5}Fe_{12-y}O_{19-\delta}$ 싱글 헥사페라이트는 1300° C 에서 뒤틀림을 하였고 샘플이 y=0.25 에서 La, Sr 결정구조에서 철의 이온의 변화에 따라서 반경이 변함을 알 수 있습니다. 샘플 평균 사이즈는 y 의 변화에 따라서 약간의 감소를 보여주었고 포화자성상태는 y 가 증가함에 따라서 약간의 증가세를 보여주고 있습니다. 가장 높은 자성값은 72.8emu/g 그리고 3300Oe 임을 알 수 있었고 $Sr_{0.5}La_{0.5}Fe_{11.5}O_{19-\delta}$(y=0.5) 인 샘플이 1325° C 에서 2 시간 방치한 샘플이 가장 적절하다는 것을 알 수 있습니다.

정리한다면, 싱글 형상은 $Sr_{0.5}La_{0.5}Fe_{12-y}O_{19-\delta}$ 헥사페라이트는 $0 \leqq y \leqq 0.5$ 인 새로운 샘플을 제조하였고, 영구적인 자성(*Ms*=70emu/g) 응용분야에 대한 새로운 시작을 하였음을 알 수 있습니다.

키워드: 자성특성, 철 함유량, Sr-La 헥사페라이트, M-type 헥사페라이트, 고체상태 반응, 포화자성상태, 항자기성